

Published in final edited form as:

Nat Metab. 2021 August 01; 3(8): 1071–1090. doi:10.1038/s42255-021-00432-5.

Leptin brain entry via a tanycytic LepR:EGFR shuttle controls lipid metabolism and pancreas function

Manon Duquenne¹, Cintia Folgueira^{#2}, Cyril Bourouh^{#3}, Marion Millet^{#4}, Anisia Silva^{#5}, Jérôme Clasadonte^{#1}, Monica Imbernon¹, Daniela Fernandois¹, Ines Martinez-Corral¹, Soumya Kusumakshi⁶, Emilie Caron¹, S. Rasika¹, Eleonora Deliglia¹, Nathalie Jouy^{1,12}, Asturo Oishi⁵, Massimiliano Mazzone⁷, Eric Trinquet⁸, Jan Tavernier⁹, Young-Bum Kim¹¹, Stéphane Ory⁴, Ralf Jockers⁵, Markus Schwaninger¹⁰, Ulrich Boehm⁶, Ruben Nogueiras², Jean-Sébastien Annicotte³, Stéphane Gasman^{4,&}, Julie Dam^{5,&}, Vincent Prévot^{1,&*}

¹Univ. Lille, Inserm, CHU Lille, Laboratory of Development and Plasticity of the Neuroendocrine Brain, Lille Neuroscience & Cognition, UMR-S1172, EGID, DISTALZ, F-59000 Lille, France

²CIMUS, Universidade de Santiago de Compostela-Instituto de Investigación Sanitaria, Santiago de Compostela, 15782, Spain- CIBER Fisiopatología de la Obesidad y Nutrición (CIBERobn), 15706, Spain

³Univ. Lille, Inserm, CHU Lille, Institut Pasteur de Lille, CNRS, U1283 - UMR 8199 - EGID, F-59000 Lille, France

⁴Centre National de la Recherche Scientifique, Université de Strasbourg, Institut des Neurosciences Cellulaires et Intégratives, F-67000 Strasbourg, France

⁵Institut Cochin, Inserm U1016, CNRS UMR 8104, University Paris Descartes, Sorbonne Paris Cité, Paris, France

⁶Experimental Pharmacology, Center for Molecular Signaling (PZMS), Saarland University School of Medicine, 66421, Homburg, Germany

⁷Laboratory of Tumor Inflammation and Angiogenesis, Center for Cancer Biology, VIB, Department of Oncology, KU Leuven, Leuven, B3000, Belgium

⁸Cisbio Bioassays, Parc Technologique Marcel Boiteux, BP84175, F-30200 Codolet, France

⁹VIB-UGent Center for Medical Biotechnology, Gent, Belgium

¹⁰Institute for Experimental and Clinical Pharmacology and Toxicology, University of Lübeck, Lübeck, Germany

Users may view, print, copy, and download text and data-mine the content in such documents, for the purposes of academic research, subject always to the full Conditions of use: <https://www.springernature.com/gp/open-research/policies/accepted-manuscript-terms>

*Corresponding author: Vincent Prévot, Ph.D., Inserm 1172, Bâtiment Biserte, Place de Verdun, 59045 Lille Cedex, France, Tel : +33 612-90-38-76, Fax : +33 320-53-85-62, vincent.prevot@inserm.fr.

&These authors jointly supervised this work

Authors Contributions

M.D., C.F., C.B., M.M., A.S., J.C., M.I., D.F., I.M.-C., S.K., E.C., E.D., N.J., A.O. and S.O. carried out the experiments. M.M., J.T., E.T., M.S., S.K. and U.B. generated tools, vectors and animal models. Y.-B.K., R.J., M.S., U.B., R.N., J.-S.A., S.G., J.D. and V.P. designed and planned the study. All authors discussed the results and M.D., S.R., S.G., J.D. and V.P. wrote the manuscript.

Competing Interests

The authors have no competing interests to declare.

¹¹Division of Endocrinology, Diabetes, and Metabolism, Beth Israel Deaconess Medical Center and Harvard Medical School, Boston, MA, USA

¹²Flow core Facility, Bioluminescence Imaging Center of Lille, campus HU, UMS2014-US41, F-59000 Lille, France

These authors contributed equally to this work.

Summary

Metabolic health depends on the brain's ability to control food intake and nutrient use versus storage, processes that require peripheral signals such as the adipocyte-derived hormone, leptin, to cross brain barriers and mobilize regulatory circuits. We have previously shown that hypothalamic tanycytes shuttle leptin into the brain to reach target neurons. Here, using multiple complementary models, we show that tanycytes express functional leptin receptor (LepRb), respond to leptin by triggering Ca²⁺ waves and target-protein phosphorylation, and that their transcytotic transport of leptin requires the activation of a LepR:EGFR complex by leptin and EGF sequentially. Selectively deleting LepR in tanycytes blocks leptin entry into the brain, inducing not only increased food intake and lipogenesis but glucose intolerance through attenuated insulin secretion by pancreatic β -cells, possibly via altered sympathetic nervous tone. Tanycytic LepRb:EGFR-mediated transport of leptin could thus be crucial to the pathophysiology of diabetes in addition to obesity, with therapeutic implications.

Introduction

Type 2 diabetes (T2D) is a common multigenic disorder affecting almost 10% of the world's population ¹. However, its characteristics are not homogeneous across the globe. In Asia, for example, T2D develops more rapidly and in individuals who are younger and have a lower body-mass index (BMI) than in other parts of the globe ². Additionally, while Asian population studies suggest that decreased insulin production by β -cells is crucial for T2D development, in other ethnicities, including Europeans, impaired insulin sensitivity, i.e. modulation of glucose levels in response to circulating insulin, is a prerequisite for incident diabetes ^{2,3}.

Leptin is a 16-kDa adipocyte-derived peptide hormone. It functions as an afferent signal in a negative feedback loop that not only controls feeding and maintains energy homeostasis ⁴⁻⁹, but also regulates glucose metabolism ^{10,11} and substrate fluxes ^{12,13} by activating leptin receptor (LepR) signaling in the brain. How circulating leptin is transported into the central nervous system to reach target neurons remains enigmatic. However, increasing evidence points to the median eminence (ME), a circumventricular organ in the basal hypothalamus adjacent to the arcuate nucleus (ARH), as a key entrance point for leptin into the metabolic brain ¹⁴⁻¹⁶.

Thanks to the porous "fenestrated" endothelium of the underlying pituitary portal capillaries, which replaces a traditional blood-brain barrier (BBB), the ME acts as a brain window at which circulating signals, including metabolic hormones, may diffuse into the brain ^{17,18}. Among the metabolic-hormone-responsive neuronal populations in this region, those of the

ventromedial ARH (vmARH)^{17,19} and neurons extending dendrites into the ME can directly sense this local blood-borne information²⁰. However, passive diffusion of metabolic signals into the ME is limited in extent^{17,19}, and tanycytes, specialized glial cells lining the floor of the third ventricle (3V), form a blood-cerebrospinal-fluid (CSF) barrier that prevents these circulating signals from reaching deeper hypothalamic structures through the CSF^{14–16}. Consequently, to cross this barrier and reach remoter targets such as dorsomedial ARH (dmARH) neurons, these signals require an active transport mechanism^{21,22}.

In a previous study, we showed that tanycytes, whose end-feet contact fenestrated capillaries below the ME, themselves internalize and shuttle extravasating blood-borne leptin into the CSF in an ERK-dependent manner²³. However, the involvement of LepR in this transport has remained unclear, with some authors questioning tanycytic LepR expression^{24,25}.

Here, using multiple *in vitro* and *in vivo* approaches and mouse models, we demonstrate that tanycytes indeed express functional LepR, which is required for the transcytotic transport of peripheral leptin into the CSF, a process that appears vital to the central control of pancreatic lipid accumulation, β -cell function and subsequent glucose homeostasis.

Results

LepR is expressed and active in ME tanycytes

To verify LepR expression by ME and ARH tanycytes, we first used the powerful RNAscope approach to visualize the long and short forms of LepR, LepRb and LepRa, respectively. Interestingly, while both isoforms occurred in tanycytic cell bodies lining the ventricular wall, this expression was relatively weak compared to the overwhelmingly high expression seen in leptin-responsive ARH neurons, explaining the failure of less sensitive methods to detect tanycytic LepR expression without resorting to cell isolation (Supplementary Figure 1A). Searching for novel tools capable of reliably detecting LepR protein in order to confirm its presence in ME tanycytes, we next characterized the biologically-active allosteric antibody XPA, recently developed to target mouse LepR²⁶. Using isolated fragments, we mapped the specific epitope of XPA to the extracellular cytokine receptor homology 1 (CRH1) domain of mouse LepR (Figure 1A; Supplementary Figure 1B), outside the orthosteric leptin-binding site of the CRH2 domain (Figure 1A, 1B). LepR BRET biosensors indicated that XPA could induce LepR oligomerization and conformational changes, although different from those promoted by the natural ligand (Figure 1C). Like leptin (50nM), 100nM XPA consistently triggered STAT3 signaling in HEK293, N46, HeLa and CHO cells transfected with LepRb (Figure 1D; Supplementary Figure 1C), as well as ERK signaling in HEK293 cells (Figure 1D). XPA also induced STAT3 phosphorylation in primary tanycyte cultures (Figure 1E), which we have previously shown to express LepR and internalize fluorescently labeled leptin²³, indicating that XPA is in fact a vital marker for activated and internalized LepR. Accordingly, a 5 min co-application of fluorescent leptin (125nM) and fluorescent XPA (30nM) to primary tanycyte cultures showed that all cells that internalized leptin also internalized XPA, and 50-60% of endocytosed leptin colocalized with XPA (Figure 1F), indicating that these cells expressed LepR and internalized it following leptin binding. To confirm tanycytic LepR expression *in vivo*, we intravenously administered XPA (2 nmol/animal) or vehicle to mice 2 min before sacrifice.

At this short interval, XPA colocalized with vimentin-immunoreactive tanycytic cell bodies and processes arching down to the fenestrated capillary plexus of the ME (Figure 1G).

In our quest for further indisputable evidence of functional LepR expression in ME tanycytes, we assessed whether tanycytes, like hypothalamic neurons, could respond to leptin by initiating Ca^{2+} signaling^{27,28}. To selectively target tanycytes, we generated mice expressing the calcium biosensor GCamp3 under the *Trpm5* promoter, which is selectively expressed in tanycytes in the ME and present in the majority of this population (Figure 1H)²⁹, by crossing *Trpm5::Cre* mice with those allowing Cre-dependent GCamp3 expression. Puffing 6 μM leptin onto the ventricular wall of living brain slices from these animals against the perfusion flow resulted in increased $[\text{Ca}^{2+}]_i$ in ME tanycytic cell bodies on live imaging (Figure 1H, 1I). Bath-application of 6 μM of the point-mutated leptin LAN (L39A/D40A/F41A), a leptin competitive antagonist that binds LepR but blocks its activity, prior to puffing leptin inhibited the leptin-induced $[\text{Ca}^{2+}]_i$ increase in tanycytes (Figure 1I, 1K), suggesting that LepR activation is required for this signaling cascade. To further test the actual involvement of LepR in this process, we generated mice with a selective LepR knockout in cells expressing the *Trpm5* promoter. In these *Trpm5::Cre; LepR^{loxP/loxP}; GCamp3^{loxP/STOP/loxP}* mice (*Gcamp3^{Trpm5}; LepR^{Trpm5KO}* mice), puffing leptin failed to induce $[\text{Ca}^{2+}]_i$ in tanycytes (Figure 1J, 1K). However, puffing 10 mM ATP, a well-known and potent activator of tanycytic calcium waves^{31,32}, readily elevated $[\text{Ca}^{2+}]_i$ in both LAN-treated and knockout brain slices, testifying to cell viability (Figure 1L, Supplementary Figure 2). Together, these data unequivocally show that tanycytes *in vivo* express active LepR, which mediates leptin-induced $[\text{Ca}^{2+}]_i$ changes.

EGFR-LepRb signaling is needed for tanycytic leptin transport

To characterize how tanycytes transport blood-borne leptin into the CSF and to distant hypothalamic sites, we next studied the transcytosis of fluorescent leptin in primary tanycyte cultures. As early as 2 min after internalization of fluorescent bioactive leptin, fluorescence was detected in EEA1-immunoreactive early endosomes (Figure 2A), where it accumulated for the first 10 min. Fluorescent leptin subsequently exited this subcellular compartment, as indicated by the decreasing intensity and extinction of fluorescence (Figure 2B, 2C, Supplementary Figure 3A) and leptin release into the medium (Figure 2D). Similarly, fluorescent LAN, which binds but cannot activate LepR, was also internalized (Supplementary Figure 3B) and reached early endosomes (Supplementary Figure 3D).

However, the overall intensity of intracellular LAN fluorescence was constant over time (Supplementary Figure 3B), and LAN remained sequestered in EEA1-immunoreactive compartments (Figure 2E, Supplementary Figure 3C–D). These results suggest that LepR signaling is not required for leptin uptake, but is required for internalized leptin to complete its transcytotic route across tanycytes into the CSF.

Next, since this transcytosis could be mediated by the leptin signaling cascade, characterized by the rapid activation of a series of tyrosine kinases (TK) and serine/threonine protein kinases (STK), we performed kinome profiling in tanycytes using the PamGene array to explore the differential activity of 140 tyrosine- and serine/threonine-containing peptides that are the targets of most known kinases, in the presence or absence of 125nM leptin

for various times. The EGFR pathway was significantly phosphorylated 2 min after leptin treatment (Figure 2F) and MAP kinases, including ERK, 2 15 min after leptin treatment (Supplementary Figure 3E). We have previously reported that ERK activation is required for leptin release by tanycytes *in vitro*, and that altered hypothalamic leptin shuttling in diet-induced obese mice can be rescued by activating ERK using potent inducers such as EGF²³. Here, the novel and unexpected finding that tanycytic EGFR itself is *trans*-activated by leptin suggests a possible molecular pathway underlying our observations.

In vivo, EGFR immunoreactivity was detected in both tanycytic cell bodies and distal processes contacting ME fenestrated capillaries (Supplementary Figure 4A). Polymerase ligation assay (PLA) using XPA demonstrated the extensive physical interaction of EGFR and LepRb in both cellular compartments, a phenomenon blunted in *Trpm5::Cre; LepR^{loxP/loxP}* mice (Figure 2G), suggesting that LepRb:EGFR signaling in tanycytic end-feet may play a role in transporting leptin once captured from the bloodstream. Intriguingly, co-transfection experiments in HEK293 cells confirmed that EGFR was immunoprecipitated with LepR, suggesting that they interacted physically even in the absence of a ligand (Figure 2H). To study the effect of ligand binding on the proximity between leptin and EGF and their cognate receptors within the LepR:EGFR complex, we next used Time-Resolved Fluorescence Resonance Energy Transfer (TR-FRET) in living HEK293 cells (Supplementary Figure 3F). Using targeted fluorescently-labeled SNAP receptors (energy donor, Terbium (**Tb**)) and ligands (energy acceptor, **d2**), TR-FRET signals the presence of a ligand at 10 nm from a specific and unique receptor within a heteromeric receptor complex³³. Because leptin does not bind to EGFR, the incubation of fluorescent leptin-d2 even at high concentrations with fluorescent SNAP-EGFR did not yield any TR-FRET signal (Figure 2I, Supplementary Figure 3F). However, co-expression of unlabeled LepR in fluorescent SNAP-EGFR-expressing cells in the presence of leptin-d2 led to a significant and specific TR-FRET signal, demonstrating the close proximity between SNAP-EGFR, LepR and leptin-d2 (Figure 2I, Supplementary Figure 3F). This leptin-d2 binding to the SNAP-EGFR:LepR complex increased and reached saturation in a concentration-dependent manner, with an affinity ($K_D(\text{SNAP-EGFR:LepRb}) = 0.42 [0.26-0.49] \text{ nM}$) similar to that of leptin binding to isolated LepR³⁴ (Figure 2I). EGF binding to EGFR did not modify the affinity of leptin binding to the LepR:EGFR complex (Figure 2I), but the significantly higher Bmax of the saturation curve indicates that it likely induced a conformational change in LepR within the complex (Figure 2I; Supplementary Figure 3G). Similarly, cells expressing EGFR and fluorescent SNAP-LepR that were stimulated by EGF-d2 (Supplementary Figure 3H) emitted a specific TR-FRET signal, reflecting a SNAP-LepR:EGFR:EGF-d2 interaction (Supplementary Figure 3I). The faint TR-FRET signal between SNAP-LepR and EGF-d2 in the absence of heterologous EGFR may have arisen from weak interaction between SNAP-LepR and endogenous EGFR. Model-fitting of the saturation curve suggests that EGF-d2 interacted with EGFR within the LepR:EGFR complex with the same affinity ($K_D(\text{SNAP-LepRb:EGFR}) = 2.1 [1.6-2.5] \text{ nM}$) as with isolated EGFR alone ($K_D(\text{SNAP-EGFR}) = 3.2 [2.4-3.7]$) (Supplementary Figure 3J). In line with leptin-d2 or EGF-d2 binding to their cognate receptors within the complex, the proximity of fluorescent leptin-Tb to EGF-d2 was only detected when LepR and EGFR were co-expressed (Supplementary Figure 3K, 3L), suggesting the formation of a quaternary complex, Leptin:LepR:EGFR:EGF, in these cells.

In isolated tanycytes, combined leptin-EGF treatment enhanced EGFR and ERK phosphorylation, supporting the intricate collaboration between these two receptors in the tanycytic ERK signaling pathway (Figure 2J). Accordingly, EGF potentiated leptin:LepR activation of ERK signaling in HEK293T cells, a reaction blunted by pre-treating cells with the EGFR kinase inhibitor, AG1478 (Figure 2K). Conversely, the inhibition of MEK1/2, the upstream activators of ERK, using U0126 led to fluorescent leptin accumulation in tanycytic early endosomes and blunted its release (Figure 2D), thus phenocopying fluorescent LAN, which does not activate LepR (Figure 2E, Supplementary Figure 3B-3D). We next verified whether directly activating EGFR-ERK signaling could bypass this LAN blockade in the tanycytic early-endosome compartment. EGF treatment (1.5nM) strikingly restored fluorescent LAN trafficking downstream of early endosomes (Figure 2E) and its probable release by tanycytes, suggesting that EGFR activation occurs downstream of LepR activation (Supplementary Figure 3C). Together, these data indicate that the tanycytic transcytosis of leptin, which allows it to reach the CSF and distant hypothalamic tissues, requires LepR-EGFR-ERK signaling.

LepR-EGFR-mediated leptin hypothalamic entry controls fat mass

To examine the role of LepR in adult tanycytes, we used TAT-Cre injection into the 3V of *LepR*^{loxP/loxP} mice. TAT-Cre infusion (2 μ l) into the 3V (1.27 μ g/ μ l over 15 min) of *tdTomato*^{loxP-STOP,loxP} reporter mice caused genetic recombination in about 60% of ME tanycytes (Supplementary Figure 5A, 5B), but not those of the area postrema, a brainstem circumventricular organ also involved in energy homeostasis³⁵ (Supplementary Figure 5C). In contrast, TAT-Cre infusion into the fourth ventricle (4V) targeted both ME and area postrema tanycytes (Supplementary Figure 5C), while TAT-Cre infusion into the lateral ventricle was ineffective in targeting ME tanycytes (Supplementary Figure 5A, 5B). FACS isolation of Tomato-positive ependymal cells from microdissected dorsal and ventral aspects of the 3V, enriched in ciliated ependymocytes and tanycytes, respectively (Supplementary Figure 5D), followed by real-time PCR readily detected LepR expression in the tanycyte-enriched population but not classic ependymocytes (Supplementary Figure 5E). Accordingly, Tomato-positive ME tanycytes after TAT-Cre infusion in *tdTomato*^{loxP-STOP,loxP}; *Lep*^{loxP/loxP} mice (Figure 3A) displayed significantly diminished expression of both short forms of LepR as well as LepRb in these cells, when compared to Tomato-positive tanycytes from *tdTomato*^{Tan}; *LepR*^{+/+} (Figure 3B, 3C). Interestingly, mRNA for *Socs3*, a known leptin-responsive transcriptional target³⁶, also appeared to be downregulated in Tomato-positive cells from *tdTomato*^{Tan}; *LepR*^{TanKO} mice (Figure 3D). Importantly, *LepR* and *Socs3* mRNA levels were not downregulated in Tomato-negative cells (Figure 3B-3D). The TAT-Cre-mediated loss of tanycytic *LepR* expression was also accompanied by a dramatic decrease in the PLA signal reporting the physical association between LepRb and EGFR (Figure 2G), as seen in *Trpm5::Cre*; *LepR*^{loxP/loxP} mice.

Interestingly, mice lacking LepR in ME tanycytes ate more (Supplementary Figure 6A), specifically in the morning after lights-on (Figure 3E), and gained significantly more weight (Figure 3F) than either vehicle-injected controls with normal tanycytic LepR expression or TAT-Cre-injected heterozygous mice (*LepR*^{TanHet}). This weight gain was associated with a 3-fold increase in fat mass 12 weeks after deleting tanycytic *LepR* (Figure 3G), but

with a concomitant loss of lean mass (Figure 3H) such that net body-mass gain remained moderate (Supplementary Figure 6B). At 12 weeks post-TAT-Cre injection, *LepR*^{TanKO} mice showed a significant increase in visceral (Figure 3I) but not subcutaneous fat mass *loxP/loxP* mass (Figure 3J) when compared to vehicle-injected *LepR*^{loxP/loxP} littermates. Surprisingly, this weight gain was independent of hyperphagia, since *LepR*^{TanKO} mice pair-fed with controls gained the same weight as *LepR*^{TanKO} mice fed *ad libitum* (Figure 3K, 3L). Using an indirect calorimetric system to characterize this change, we found that weight gain in *LepR*^{TanKO} mice was associated with an increased respiratory exchange ratio (RER) during the light phase both 4 weeks (Supplementary Figure 6A2) and 12 weeks after TAT-Cre injection (Figure 3M, 3N). This phenomenon was conserved under the pair-fed condition (Figure 3K), where *LepR*^{TanKO} mice kept gaining more weight than *LepR*^{loxP/loxP} littermates (Figure 3L), even though energy expenditure (Supplementary Figure 6A3, 6C) and locomotor activity (Supplementary Figure 6A4, 6D) remained unchanged. Similar changes were observed when, instead of TAT-Cre infusion, tanycytes *in vivo* were transduced with a viral vector expressing Cre under the control of the tanycyte-specific *Dio2* promoter³¹ (Supplementary Figure 6A5-A8).

Interestingly, in accordance with the marked increase in fat mass, circulating leptin levels appeared higher as early as 4 weeks after TAT-Cre-mediated *LepR* deletion in tanycytes (Figure 3O). Taking into account the close relationship between LepR and EGFR and the likely *trans*-activation of LepR to some extent by endogenous EGF (Figure 2, Supplementary Figure 3), we therefore also measured circulating EGF levels in *LepR*^{TanKO} mice, to determine whether deficient LepR signaling would trigger compensatory changes in the EGF-EGFR signaling pathway. Surprisingly, circulating EGF levels, which were readily detectable, were increased in *LepR*^{TanKO} mice (Figure 3P). However, they were unchanged in wild-type mice given a high-fat diet for 8 weeks as compared to chow-fed controls (Figure 3Q), suggesting that the increased EGF levels in *LepR*^{TanKO} mice were not related to their higher circulating leptin levels per se (Figure 3O), but rather to central phenomena linked to deficient LepR signaling.

Increased food intake after overnight feeding (Figure 3E) despite elevated adiposity (Figure 3G, 3I) and circulating leptin levels in *LepR*^{TanKO} mice (Figure 3O) raised the possibility that these animals could be developing hypothalamic resistance to circulating leptin, associated with defective leptin transport by tanycytes, as seen early in diet-induced obesity in various animal models^{23,37}. First, to confirm that this phenomenon occurs under physiological conditions, we assessed endogenous STAT3 activation in the ARH, a surrogate for endogenous LepR activation^{22,38}, at lights-on after overnight feeding, when circulating leptin levels are at their highest³⁹. While the number of P-STAT3-immunoreactive cells lying outside the BBB in the vmARH was unaffected in *LepR*^{TanKO} mice (Supplementary Figure 7A, 7B), their number in the dmARH was diminished by about 30% when compared to *LepR*^{loxP/loxP} control littermates (Supplementary Figure 7A, 7C). We then assessed the activation of leptin-sensitive hypothalamic neurons 15 min after an intraperitoneal (i.p.) bolus of exogenous leptin. While leptin-induced P-STAT3 activation was unaffected in the vmARH (Figure 4A, 4B), it was still significantly hampered in the dmARH of *LepR*^{TanKO} mice (Figure 4A, 4C). To determine how this decreased access to peripheral leptin could impact ARH neuronal populations involved in controlling bodily homeostasis, we

analyzed the expression of several key leptin-regulated transcripts by q-PCR. In *LepR*^{TanKO} mice, transcripts for the melanocortin receptor antagonist Agouti-related peptide (*Agrp*) were significantly induced, whereas *Socs3* mRNA levels were downregulated (Figure 4D). Next, we subjected *LepR*^{TanKO} mice and their control littermates to an i.p. or intracerebroventricular (i.c.v.) injection of exogenous leptin and measured food intake 24h later (Figure 4E). While leptin injected directly into the CSF reduced feeding in both groups of mice equally, *LepR*^{TanKO} mice, unlike *LepR*^{loxP/loxP} mice, were unable to respond to i.p. leptin by decreasing food intake (Figure 4E), suggesting once again that tancytic LepR is necessary for peripheral leptin to reach leptin-sensitive neurons not in the immediate vicinity of ME fenestrated vessels. Finally, we verified that the decreased response to peripheral leptin in *LepR*^{TanKO} mice was due to an alteration in the LepR-dependent tancytic transport of blood-borne leptin into the hypothalamus by implanting microdialysis probes into the dorsomedial mediobasal hypothalamus of mutant mice and control littermates (Figure 4F). In agreement with the P-STAT3 distribution under physiological conditions (Supplementary Figure 7), basal leptin levels in this region, before any dilution effect of peripheral vehicle injection, were significantly lower in *LepR*^{TanKO} mice (0.8 ± 0.5 pg/ml) than in *LepR*^{loxP/loxP} littermates (26.5 ± 7.5 pg/ml, t-test, $p=0.0196$). Additionally, 20 min after an i.p. leptin bolus, *LepR*^{loxP/loxP} mice displayed a significant early peak in hypothalamic leptin levels before reaching an intermediate plateau and a second peak at 80 min, which were both absent in *LepR*^{TanKO} mice (Figure 4F); instead, in these mice, leptin levels merely showed a small, non-significant rise at 60 min but remained at near nadir levels otherwise (Figure 4F).

Similarly, mice in which tancytic EGFR expression was blunted by AAV1 /2-mediated *Egfr* silencing RNA expression (Supplementary Figure 4B, Figure 4G) phenocopied certain aspects of *LepR*^{TanKO} mice, notably the concomitant decrease in lean mass and increase in fat mass with no modification of body weight 8 weeks after infection (Figure 4H-4J). Like *LepR*^{TanKO} mice, these animals also showed a hampered ability to respond to i.p. leptin by decreasing food intake (Figure 4K).

Altogether, these results strongly support the view that tancytic LepR-EGFR signaling is required for blood-borne leptin transport into the hypothalamus and its anorexigenic effect, and reveals an unprecedented role for this transport in the control of body composition.

Mice lacking tancytic LepR show altered lipid metabolism

Given the increased RER in *LepR*^{TanKO} mice (Figure 3M), indicative of the increased consumption of carbohydrates over lipids to meet energy requirements⁴⁰, we next examined lipid metabolism in mice with defective leptin transport into the hypothalamus. The changes in RER and food-intake-independent body-weight gain in *LepR*^{TanKO} mice appeared to be due to decreased fatty acid oxidation (Figure 5A), associated with both increased visceral fat mass (Figure 3I) and leptinemia (Figure 3O) and elevated circulating cholesterol and triglycerides (Figure 5B), but not non-esterified free fatty acids (NEFAS) (Figure 5C). These data, together with larger white adipocytes (Figure 5D), suggest that *LepR*^{TanKO} mice show hyperlipidemia and lipid accumulation in white adipocytes.

In agreement with increased free fatty acid uptake into white adipose tissue in response to central leptin deficiency¹³, *LepR*^{TanKO} mice showed a marked increase in protein levels of lipoprotein lipase (LPL), an enzyme that promotes the uptake of circulating triglycerides, and acetyl-CoA carboxylase (Acc) and fatty acid synthase (FAS), enzymes crucial for *de novo* lipogenesis, in ependymal fat (Figure 5E, 5F). Notably, the ratio of phosphorylated Acc to total Acc was decreased in *LepR*^{TanKO} mice (Figure 5E, 5F), suggesting, in agreement with previously published data¹³, that hypothalamic leptin regulates Acc in white adipose tissue. Next, we found that the phosphorylation of the key lipolytic enzyme hormone-sensitive lipase (HSL), whose activity is also known to be regulated by central leptin signaling¹³, was lower in *LepR*^{TanKO} mice than in control littermates (Figure 5E, 5F). Overall, these results indicate that LepR deficiency in tanycytes favors lipid accumulation by promoting lipogenesis and lipid uptake while inhibiting lipolysis in white adipose tissue. Importantly, these effects were independent of feeding since they occurred in both *LepR*^{TanKO} mice fed *ad libitum* and those pair-fed with the control group.

Increased lipid accumulation was also noted in the liver of *LepR*^{TanKO} mice using oil-red staining (Figure 5G). Accordingly, liver triglyceride content was higher in these mice even when pair-fed (Figure 5H), whereas circulating triglycerides were comparable to those in *LepR*^{loxP/loxP} controls (Figure 5B). Given the absence of any marked change in the expression of enzymes involved in lipid metabolism (Figure 5I, 5J), the increased lipid accumulation in the liver of *LepR*^{TanKO} mice is likely not due to local *de novo* synthesis but indirectly to their increased weight and hyperlipidemia.

Tanycytic LepR-deficient mice develop impaired pancreatic function

Leptin has long been known to influence glucose homeostasis independently of its effect on body weight regulation^{41,42}. These effects appear to be mediated by LepR-expressing ARH neurons, since reinstating LepR expression locally in otherwise LepR-knockout animals normalizes insulinemia¹¹. In light of the altered gene expression in ARH neurons observed in our mice, we next investigated the effect of tanycytic LepR deletion on glucose metabolism. Four weeks after LepR deletion, mice appeared to have no difficulty managing exogenous glucose injections (Figure 6A). Intriguingly, however, 4 weeks after LepR deletion, despite normal glucose tolerance at this early time point (Figure 6A), *LepR*^{TanKO} mice showed higher insulin release than control *LepR*^{loxP/loxP} or *LepR*^{TanHet} mice both before (12h fasting insulin: *LepR*^{TanKO}, 0.81±0.12 µg/µl vs. *Lep*^{loxP/loxP}, 0.48±0.06 µg/µl and *LepR*^{TanHet}, 0.46±0.03 µg/µl, p = 0.03 and p = 0.04, respectively, one-way ANOVA and Tukey's multiple comparison test) and after glucose injection (Figure 6B), despite an apparently normal response to insulin (Figure 6C), suggesting a disconnect between pancreatic β-cell activity and physiological needs. This elevated insulin release by β-cells even under basal conditions phenocopies mice lacking LepR in proopiomelanocortin (POMC) neurons⁴³, concordant with an inability of ARH neurons to correctly perceive circulating leptin levels as suggested by decreased STAT3 activation after overnight feeding (Supplementary Figure 7) or exogenous leptin treatment (Figure 4A, 4C), as well as *Socs3* downregulation in the ARH of *LepR*^{TanKO} mutants (Figure 4D).

By 12 weeks after *LepR* deletion, however, *LepR*^{TanKO} mice developed impaired tolerance to exogenous glucose (Figure 6D), although their basal insulin levels were similar to those in *LepR*^{loxP/loxP} mice. This altered glucose homeostasis in *LepR*^{TanKO} mice was also correlated with a significantly lower increase in glucose-stimulated insulin levels, suggesting some degree of pancreatic dysfunction (Figure 6E). Insulin sensitivity and HOMA-IR were similar in the two genotypes (Figure 6F, 6G). To investigate possible alterations in pancreatic function in mice lacking tanycytic *LepR*, we investigated glucose-stimulated insulin secretion (GSIS) in isolated pancreatic islets from *LepR*^{TanKO} and *LepR*^{loxP/loxP} littermates. Although *LepR* deletion in tanycytes did not affect the total insulin content of islets (Figure 6H), insulin secretion from isolated islets under high-glucose conditions was severely hampered in 12-week *LepR*^{TanKO} when compared to *LepR*^{loxP/loxP} mice (Figure 6I). Gene expression analysis in islets from these mice revealed an increased expression of genes involved in glucose sensing (*Glut2*, *Gck*) and insulin maturation (*Pcsk1*) but decreased expression of β -cell identity genes such as *Pdx1* ($p=0.065$) and *MafA* (Figure 6J). *LepR*^{TanKO} islets also exhibited an increase in markers of the endoplasmic reticulum unfolded protein response (UPR^{er}) pathway, including *Atf4* ($p=0.016$), *Xpb1t* and *Chop* (Figure 6K), thought to be associated with impaired β -cell function and T2D development⁴⁴. The number of α - (glucagon-positive) and β - (insulin-positive) cells per pancreatic islet was similar in the two genotypes (Figure 6L-6N). Altogether, these data suggest that the loss of *LepR* function and the tanycytic leptin shuttle impairs glucose homeostasis and insulin secretion through the transcriptional control of key β -cell and UPR^{er} markers, and that the whole sequence of events unfolds within 3 months.

To determine whether restoring hypothalamic access to leptin could rescue β -cell function in 12-week *LepR*^{TanKO} mice, we deprived animals of food 3h before stereotaxically injecting them with 2 μ g of leptin i.c.v., shortly before lights-off. At lights-on, i.e. 12h after leptin injection in food-deprived animals, a glucose tolerance test was performed. Pre-treatment with leptin significantly rescued impaired glucose management in *LepR*^{TanKO} mice, without further depressing glycemia in *LepR*^{loxP/loxP} littermates (Figure 6O). Additionally, although glucose-stimulated insulin secretion at 15 min was lower in *LepR*^{TanKO} mice than in *LepR*^{loxP/loxP} littermates in the absence of leptin pre-treatment (Figure 6E), central leptin administration significantly increased insulin secretion 15 min after glucose injection in both mutant and control mice, compensating for defective tanycytic function (Figure 6P). These results demonstrate that the hypothalamic actions of tanycyte-transported leptin are vital for the acute control of β -cell function directly by the brain, likely through the connection of leptin-sensing ARH neurons to the pancreas via the autonomic nervous system⁴³, and raise the intriguing possibility that defects in the tanycytic leptin shuttle may also play a critical central role in the pathophysiology of diabetes.

Sympathetic tone mediates effects of impaired central leptin access

The central effects of leptin on glucose homeostasis appear to involve the melanocortin system⁴³, whose receptor antagonist AgRP is altered in our *LepR*^{TanKO} mice above (Figure 4D). This impinges upon the sympathetic nervous system^{45,46}, which also mediates the central effects of leptin on white adipose tissue lipid metabolism¹³. We therefore assessed circulating noradrenaline levels in *LepR*^{TanKO} mice (Figure 4E, 4F), and found that they

were reduced, suggesting an overt decrease in sympathetic tone when compared to *LepR*^{loxP/loxP} littermates (Figure 7A). Interestingly, pancreatic islets in *LepR*^{TanKO} animals expressed more α 2A adrenergic receptors, known for their inhibitory action on pancreatic insulin secretion^{47,48}, than their littermates, without affecting β 2 adrenergic receptor expression (Figure 7B). Furthermore, when *LepR*^{TanKO} mice were subjected to a 2h exposure to cold (4°C), they experienced a drop in rectal temperature (Figure 7C) associated with defective cold-induced noradrenaline secretion (Figure 7D). Together, these results suggest a possible mechanism whereby decreased leptin access to hypothalamic neurons controlling bodily homeostasis alters overall sympathetic tone, in turn affecting peripheral glucose and lipid metabolism. Because previous studies have shown that brain-pancreas and brain-adipose tissue connections involve leptin signaling through the melanocortin system^{43,49}, it is tempting to speculate that the main hypothalamic neuronal population affected by defective leptin shuttling into the brain is that of AgRP-expressing ARH neurons, which mediate melanocortin signaling.

Tanycytic *LepR* knockout blunts the response to fasting

Given our previous demonstration of tanycytic involvement in the adaptive response to fasting²², and because leptin has long been known to play important physiological roles during starvation, we next tested the ability of peripheral leptin treatment (1mg/kg/12h) to attenuate the adaptive neuroendocrine response to 24h fasting in *LepR*^{TanKO} mice. While leptin repletion after starvation had no effect on blood glucose, it reduced food intake over the first 4h and 12h of refeeding and consequently reduced weight gain after 24h in *LepR*^{loxP/loxP} but not in *LepR*^{TanKO} mice (Table 1). Interestingly, while 24h fasting dramatically increased corticosterone levels in *LepR*^{loxP/loxP} mice, a phenomenon normalized by leptin replacement, it left corticosterone levels in *LepR*^{TanKO} mice unchanged (Table 1).

Overall, our results strongly suggest that in the absence of the tanycytic leptin shuttle, the brain loses its ability to properly respond to physiological challenges and thus to restore bodily homeostasis.

Discussion

Leptin, a hormone secreted by adipocytes, plays a fundamental role in regulating energy homeostasis by controlling food intake and energy expenditure⁴⁻⁹. To achieve its central effects, leptin needs to cross the BBB and access specific leptin-sensitive neurons in the hypothalamus and elsewhere, a process mediated by tanycytes²³. Our results convincingly show that, in contrast to recent studies that question *LepR* expression in tanycytes²⁵, *LepR* is not only expressed but is functionally active in hypothalamic ME tanycytes, and transports leptin into the hypothalamus in a leptin- and EGF-dependent manner by forming a complex with EGFR.

The assumption that *LepR* is not expressed in tanycytes could be due to the fact that, like astrocytes, these specialized hypothalamic glia do not express commonly used Cre-dependent reporter genes²⁴ or that most alternative detection techniques used so far are not sensitive enough²⁵. Additionally, in the tamoxifen-inducible Cre-driver mouse lines used by others²⁵, *LepR* gene accessibility in tanycytes may be impaired, since tamoxifen

is known to alter chromatin architecture⁵¹, interfere with estrogen receptor activity and itself impact metabolism⁵². Here, we overcame these technical problems by an array of methods detecting not only the presence of LepR protein in ME tanycytes but also its function. Additionally, we demonstrate that tanycytic LepR signaling is critical for the transcytotic mechanism by which blood-borne leptin is shuttled into the hypothalamus, and that leptin-mediated LepR activation causes the early activation of EGFR, which we had serendipitously found to rescue diet-induced obese animals from central resistance to peripheral leptin²³. This leptin-LepR-dependent EGFR activation in tanycytic processes contacting the fenestrated endothelium of pituitary portal capillaries *in vivo* is required for leptin release from early endosomes by triggering the downstream ERK signaling pathway. Furthermore, while LepR and EGFR appear to form a complex capable of binding both leptin and EGF, EGFR activation by EGF potentiates the effects of leptin on ERK activation while leaving STAT3 activation unaffected. The kinetics of EGFR and ERK activation by leptin in primary tanycytes, with the early leptin-induced phosphorylation of EGFR followed by ERK phosphorylation at 15 min, is reminiscent of that reported in gastric cancer cells⁵³. Although we detected circulating EGF in our animals, tanycytic EGFR activation could also involve *trans*-activation processes similar to those observed in cancer cells⁵³ and also known to occur in tanycytes^{54,55}.

Leptin signaling in the brain also exerts specific and complementary peripheral effects on adipose tissue through the regulation of nutrient partitioning by decreasing the expression of key *de novo* lipogenic enzymes and stimulating lipolysis^{7,13}. Interestingly, in addition to its mild consequences on body weight, deleting tanycytic LepR expression in the ME of adult mice increases food intake, favors the disproportionate use of carbohydrates, thus favoring lipid accumulation, dramatically alters body composition by promoting fat mass to the detriment of lean mass, and also impairs the brain's ability to control glucose homeostasis in association with altered pancreatic β -cell function and sympathetic tone.

The capacity of leptin to regulate these diverse metabolic parameters resides in LepR-expressing ARH neurons, namely POMC and AgRP neurons, known to be involved in controlling adipose tissue lipogenesis¹³ and glucose homeostasis¹¹ in response to this adiposity signal. For instance, LepR deletion in either neuronal population leads to moderate obesity, while its deletion in both populations combined has clear cumulative effects on adiposity despite a comparable effect on food intake^{56,57}. The fact that our mice mimic this metabolic phenotype suggests that LepR depletion in tanycytes precludes leptin access to POMC and AgRP neurons and its subsequent actions. Supporting this hypothesis, LepR removal from tanycytes severely hampers the ability of endogenous or exogenous leptin to reach the mediobasal hypothalamus and activate leptin-sensitive dmARH neurons, and upregulates transcripts for the melanocortin receptor antagonist *Agrp*, while downregulating *Socs3*, a known leptin-responsive gene³⁶. Interestingly, the melanocortin system is involved not only in glucose homeostasis^{11,43,58} but also in sympathetic nervous system regulation of lipid metabolism in white adipose tissue^{13,49}, and both nadir and cold-induced circulating noradrenaline levels are reduced in mice lacking tanycytic LepR. In light of these findings, we propose that deficient leptin-regulated POMC and AgRP neuronal activity in the dmARH alters their use of melanocortin signaling^{59,60} to communicate with autonomic nervous system neurons in the brainstem and spinal cord^{45,61}, and thus their control

of peripheral tissues^{7,62}. In keeping with this hypothesis, we found decreased insulin secretion by pancreatic β -cells in mice lacking tanycytic LepR in association with increased expression of α 2A adrenergic receptors, in agreement with previous studies showing both decreased glucose tolerance and insulin exocytosis by β -cells when these receptors are activated⁴⁷. Additionally, in humans, a polymorphism leading to the overexpression of ADRA2A is associated with increased risk of developing T2D⁴⁸. Our results fill several mechanistic gaps in our understanding of leptin action: i) blood-borne leptin reaches dmARH neurons through a singular route involving transcytotic transport by ME tanycytes, which depends on activation of a LepR:EGFR complex and ERK signaling, ii) leptin then stimulates dmARH neurons controlling the melanocortin system and sympathetic outflow, and iii) this diminishes adipose tissue lipid storage and controls glucose homeostasis by shaping the function and plasticity of α 2A adrenergic-receptor-expressing pancreatic islet cells. Conversely, alterations in tanycytic leptin transport manifest as decreased sympathetic tone, increased visceral adiposity, hepatic steatosis and glucose intolerance with pancreatic dysfunction.

Intriguingly, regardless of whether LepR or EGFR signaling is defective, the fat-mass gain observed in our experiments occurs concomitantly with a loss of lean tissue, with the result that overall weight gain remains limited. Because fatty acid uptake by muscles is inversely related to visceral fat⁶³, one possible explanation is that the increased abdominal fat and decreased fatty acid oxidation in fat tissue may be secondary to, rather than a cause of, reduced lean mass. However, under resting conditions, decreased fatty acid uptake and oxidation in muscles are generally associated with insulin resistance (see for review⁶⁴), which does not occur in mice deficient in tanycytic LepR. This phenomenon associating obesity with sarcopenia (sarcobesity) is reminiscent of that commonly seen during aging^{65,66} and may promote related conditions such as diabetes and frailty⁶⁷. A recent study has shown that in mouse models of hyperglycemia and T2D due to defective β -cell function, intertissue crosstalk and amino-acid catabolism leads to skeletal muscle atrophy⁶⁸. Further studies are required to explore this pathway in mice with altered tanycytic LepR:EGFR signaling to determine its impact on aging.

Human studies show that T2D develops in subjects exhibiting insulin hypersecretion in normoglycemic and prediabetic phases in order to keep glycemia near normal in a context of chronic nutrient surfeit and obesity-associated insulin resistance, until they reach a threshold at which this compensatory β -cell response becomes unsustainable⁶⁹. Compensating for insulin resistance by increasing insulin secretion usually requires both augmented β -cell function and β -cell mass, the latter being stimulated by increased nutrient supply, including glucose and free fatty acids⁷⁰. However, diabetes is a heterogeneous disease⁷¹, and an alternative pattern characterized by a β -cell functional deficit could predominate in some ethnic groups. This phenotypic stratification is seen in a Japanese study in which 50% of patients with dysfunctional β -cells progressed to T2D onset, as compared to only 14% of patients with insulin resistance⁷². Intriguingly, an epidemiological study of Korean patients with T2D revealed impaired insulin secretion and insulin resistance 10 years before disease onset, and impaired β -cell compensation with an abrupt decrease in insulin secretion during the last 2 years before onset³, underscoring the central role of β -cell dysfunction in T2D pathogenesis in Asian populations. The existence of two patterns of disease progression

can also be seen from the fact that East-Asian T2D patients have a much lower BMI than European patients but more intra-abdominal fat for similar BMI values². In our current model, the attenuation of tancytic leptin transport leads to an initial increase of insulin secretion despite the absence of insulin resistance, followed over time by impaired glucose-stimulated insulin secretion against a backdrop of increased visceral fat but normal insulin sensitivity. This phenomenon can be seen in isolated pancreatic islets despite their apparently unaltered size and organization, suggesting modified β -cell functional integrity instead, thus mimicking the principal human phenotype described above. Interestingly, this functional deficit could be reversed by reestablishing central control by infusing leptin directly into the cerebral ventricles.

To summarize, the study of our *LepR*^{TanKO} mouse model has unmasked two important aspects of leptin action: i) the molecular and cellular mechanisms regulating the physiological access of leptin to leptin-responsive neurons in the brain, i.e. the LepR-EGFR-ERK-mediated transcytotic transport of blood-borne leptin into the hypothalamus by tancytes, and ii) the link between deficient tancytic leptin transport and the pathophysiology of pancreatic β -cell failure and lipid dysmetabolism in the context of moderate overweight and sarcobesity. Together, these findings shed light on the central control of peripheral lipid and glucose homeostasis by leptin, and create new therapeutic avenues for metabolic disorders.

Methods

Animals

All C57Bl/6J adult male mice were housed under specific pathogen-free conditions in a temperature-controlled room (21-22°C) with a 12h light/dark cycle and 40% humidity, and *ad libitum* access to food and water. *tdTomato*^{loxP-STOP-loxP} (IMSR Cat#JAX007914, RRID:IMSR_JAX007914) and GCamP3^{loxP-STOP-loxP} (IMSR Cat#JAX025406, RRID:IMSR_JAX025406) reporter mice and *LepR*^{loxP-STOP-loxP} mice (IMSR Cat#JAX008327, RRID:IMSR_JAX008327)⁷³ were purchased from the Jackson Laboratories (Bar Harbor, ME). *Tpm5::Cre* mice were engineered by Dr. Ulrich Boehm (University of Saarland, Homburg, Germany)²⁹. All experiments and procedures involved in this study were approved by the Ethics Committee of the Universities of Lille and Santiago de Compostela, in accordance with European Union norms for experimental animals.

TAT-Cre, pAAV-Dio2-iCre-2A-GFP and AAV(1+2)-GFP-U6-m-EGFR-shRNA delivery

TAT-Cre fusion protein (1.27 mg/ml) and AA1/2 *Dio2::Cre* (0.5x10⁹ genomic particles/ μ l) were produced as detailed previously^{31,74}. AAV(1+2)-GFP-U6-m-EGFR-shRNA was produced by Vector Biolabs (shAAV-258137). All products were stereotaxically infused into the third ventricle (3V)(2 μ l over 7min; anteroposterior, -1.7mm; midline, 0mm; dorsoventral, -5.6mm), lateral ventricle (LV)(Anteroposterior, -0.3mm; midline, +/-1mm; dorsoventral, -3mm) or fourth ventricle (4V)(Anteroposterior, -6mm; midline, 0mm; dorsoventral, -4mm) of 24h-fasting isoflurane-anesthetized floxed mice 1 and 3 weeks before experiments for TAT-Cre and virus injections, respectively.

Evaluation of TAT-Cre recombination efficiency

Four weeks after LV or 3V TAT-Cre infusion in *TdTomato* mice, animals were anesthetized with ketamine (8mg/kg)+xylazine (3mg/kg) before perfusion with 0.9% NaCl and 4% paraformaldehyde. Brains were collected, cryoprotected in 20% sucrose solution overnight, embedded in TissuTek (Sakura) and frozen. 16µm-thick coronal sections were cut and processed for immunofluorescence using chicken anti-vimentin (1:2000; Millipore Cat#AB5733, RRID:AB_11212377) primary and AlexaFluor-647-conjugated anti-chicken secondary antibody (1/1000; ThermoFisher Scientific Cat#A-21449, RRID:AB_2535866). Images were acquired using an AxioImager Z2 Apotome microscope (AxioCam MRm camera, Zeiss) and Zen 3.1 (blue edition) software. Eight representative ME slides/animal were coded to conceal treatment groups and tanycytes (vimentin-positive cells) divided into three groups depending on their projections (ME-ARH, ventromedial hypothalamus, dorsomedial hypothalamus). DAPI+/Tomato+/vimentin+ cell numbers was reported relative to DAPI+/vimentin+ cells bordering the 3V.

FACS-sorted Tomato-positive cell numbers were compared between microdissected samples of the ME (3V) and 4V, 1 week after infusion.

Fluorescence-activated cell sorting (FACS) and real-time PCR

FACS isolation of hypothalamic tanycytes—MEs from TAT-Cre-injected *tdTomato*^{loxP/+} and *LepR*^{oxP/loxP} *tdTomato*^{loxP/+} mice were microdissected and enzymatically dissociated (Papain Dissociation System, Worthington, Lakewood, NJ) to obtain single-cell suspensions. FACS was performed using an ARIA SORP cell sorter-cytometer and FACSDiva software v 8.0.3 (BD Bioscience, Inc). The sort decision was based on tdTomato fluorescence (excitation 561nm; detection: bandpass 675+/-20nm) compared to wild-type animals (Figure 3A). For each animal, 4000 tdTomato-positive and negative cells were sorted directly into 10µL extraction buffer: 0.1% TritonX-100 (Sigma-Aldrich) and 0.4 U/µl RNaseOUT (ThermoFisher).

Quantitative RT-PCR—For gene-expression analyses, mRNA from microdissected hypothalamic explants or FACS-sorted tanycytes was reverse transcribed using SuperScript III Reverse Transcriptase (Life Technologies) and a linear preamplification step applied to sorted cells only using the TaqMan PreAmp Master Mix protocol (P/N 4366128, Applied Biosystems). RT-PCR was carried out on the Applied Biosystems 7900HT Fast Real-Time PCR System using exon-boundary-specific TaqMan Gene Expression Assays (Applied Biosystems) (Table S1). Gene-expression data were analyzed using SDS 2.4.1 and Data Assist 3.0.1 software (Applied Biosystems).

Physiological measurements

Body composition—Body composition was measured weekly in several experiments using a Minispec LF Series (Bruker Corporation, Massachusetts). Fat and lean mass data were expressed as % body weight.

Analysis of basal metabolism—Mice were analyzed for total energy expenditure, oxygen consumption, CO₂ production, food intake and ambulatory movements (total

beam breaks/h) using calorimetric cages (TSE Systems GmbH, Germany) and standard procedures. Mice were individually housed and acclimatized to cages for 48h before measurements. Pair-fed animals received the mean weight of food eaten by the control group during the previous 24h (see below). RER and energy expenditure (EE) were calculated as reported previously^{75,76}, and fatty-acid oxidation as reported by Bruss and colleagues⁷⁷ (Equation 1).

$$\text{FA oxidation (kcal/h)} = \text{EE} \times (1 - \text{RER}/0.3) \quad (\text{Equation 1})$$

Pair-feeding—Pair-feeding experiments were performed as documented previously^{78,79}. We assessed food intake under normal conditions in LepR^{loxP/loxP} and LepR^{TanKO} mice for at least one week without experimentation/stressors, then pair-fed LepR^{TanKO} mice with the group showing lower food intake, i.e., LepR^{loxP/loxP} mice. To avoid altering results in pair-fed animals due to long fasting periods, pair-fed LepR^{TanKO} mice received 2/3 of their daily food quota just before the dark phase and 1/3 at lights-on (when mice eat less).

Glucose tolerance and insulin dosage—After overnight fasting (12h), tail blood samples for insulin measurement were taken using glass capillaries before, 15 and 30min after glucose administration. Samples were kept on ice before centrifugation (4°C, 600rpm, 15min) and serum frozen at -80°C until insulin ELISA (Mercodia). Basal blood glucose levels were measured before i.p. glucose administration (1.5mg glucose/g body weight), 15, 30, 45, 60, 120 and 150min after glucose administration using a OneTouch Verio glucometer. One cohort of animals was injected i.c.v. with recombinant murine leptin (2µg/animal; Harbor-UCLA Medical Center, California) 3h before lights-off, mice were subjected to 12h fasting, and glucose tolerance and insulin measured the next day.

Insulin response measurement—Basal blood glucose levels were measured before i.p. insulin administration (0.75UI/kg body weight), 15, 30, 45, 60, 120 and 150min after glucose administration using a OneTouch Verio glucometer in 6h-fasting mice.

In vivo leptin sensitivity test—Individually housed mice were subjected to 3h fasting in the afternoon and treated with murine leptin (3mg/kg; Harbor-UCLA Medical Center, California) or vehicle (PBS pH8.0) i.p. or i.c.v. 3h before refeeding. Body weight and food intake were measured before, 12h and 24h after treatment.

Effect of leptin on the corticosterone response—Two weeks before fasting, at lights-on, glycemia was measured and cheek blood drawn⁸⁰ to assess serum corticosterone levels in fed mice. Then, mice were individually housed, subjected to 24h fasting, and half received leptin (1mg/kg) or saline i.p. every 12h (8am and 8pm). Cheek blood samples were taken before refeeding. Food intake was measured 4h, 12h and 24h after refeeding. Corticosterone levels were quantified by ELISA (55-CORMS-E01; American Laboratory Products) following manufacturer's instructions.

Cold-exposure test

Rectal temperature was measured in mice before cheek blood samples were collected. 1h later, mice were exposed to 4°C for 2h, rectal temperature taken and blood recollected. Temperature difference before and after cold exposure was calculated, and fed and fasting serum noradrenaline concentrations quantified by ELISA (see below).

In vivo microdialysis

Nine *LepR^{loxP/loxP};tdTomato^{loxP-STOP-loxP}* mice were injected in the LV with AAV(1/2) *Dio2::Cre* (n=4) or vehicle (n=5). A microdialysis cannula (CMA8 High Cut-off, 100kDa, 1mm membrane length; CMA microdialysis AB, Sweden) was stereotaxically implanted in the mediobasal hypothalamus (antero-posterior: -1.3, lateral: -0.3, ventral: -6.1 mm) in 25-35g isoflurane-anesthetized mice with core body temperature maintained at 37°C using thermostat-controlled electrical blanket. The cannula was then perfused at 2μL/min with sterile artificial CSF (ACSF; CNS Perfusion Fluid: NaCl 147mmol/L, KCl 2.7mmol/L, CaCl₂ 1.2mmol/L and MgCl₂ 0.85mmol/L; CMA, Stockholm, Sweden) using a microinjection pump (CMA 402; CMA, Stockholm, Sweden). Following stabilization for 45min, a basal dialysate of 20min was collected. A vehicle injection (i.p., PBS pH8.0) was administered and two 20min dialysates recovered. Finally, at 60 min, leptin (i.p., 3mg/Kg in PBS pH8.0, Harbor-UCLA Medical Center, California) was administered to mice and 5 dialysates of 20min recovered. Dialysates were placed in a fraction collector (CMA/820) during the experiment and immediately stored at -80°C until analysis. At the end of the experiment, mice were decapitated and brains stored immediately in fresh 4% paraformaldehyde. 80μm-thick vibratome brain sections were counterstained with DAPI to verify probe location. Only mice in which the probe was positioned between antero-posterior -1.2 and -2.3 were included in analyses.

Leptin, EGF and noradrenaline ELISAs—Basal serum leptin concentrations in *LepR^{loxP/loxP}* and *LepR^{TanKO}* mice and leptin content in brain

microdialysates were measured using ELISA (Leptin mice MOB00; R&D systems). Serum EGF concentrations from normal-chow- or 8-week high-fat-diet-fed (#D12492; Research Diets) C57Bl/6J, *LepR^{loxP/loxP}* and *LepR^{TanKO}* mice were quantified using a mouse EGF ELISA kit (EMEGF ; ThermoFisher). Basal serum noradrenaline concentrations in *LepR^{loxP/loxP}* and *LepR^{TanKO}* mice were quantified using a noradrenaline ELISA kit (BA-E5200; Immusmol).

Brain and peripheral tissue analysis

Brain slice preparation and calcium imaging—Eight-to 12-week-old male *GCaMP3^{Trpm5}* and *GCaMP3^{Trpm5};LepR^{Trpm5}* mice were anesthetized with isoflurane, decapitated, and the brain rapidly removed and put in ice-cold oxygenated (O₂ 95% / CO₂ 5%) artificial CSF (ACSF) containing (in mM): 120 NaCl, 3.2 KCl, 1 NaH₂PO₄, 26 NaHCO₃, 1 MgCl₂, 2 CaCl₂, 10 glucose (300 mOsm, pH7.4). After removal of the cerebellum, the brain was glued and 200μm-thick coronal hypothalamic slices containing the ME and lateral walls of the 3V cut using a vibratome (VT1200S; Leica) as previously described⁸¹. Slices were allowed to recover at 35°C for 1h, placed in a submerged recording

chamber (31°C; Warner Instruments) and continuously perfused (2ml/min) with oxygenated ACSF. Tanycytes were observed with a 40x water-immersion objective using an upright Leica DM-LFSA microscope with infrared differential interference contrast (IR-DIC). GFP fluorescence was detected under blue illumination at 470 nm and images collected with an ORCA-Flash4.0 LT digital CMOS camera (Hamamatsu), using MetaMorph image acquisition software (Molecular Devices). Images were analyzed off-line using MetaMorph 7.8.12.0 (Molecular Devices) and Fiji software. Regions of interest (ROI) were drawn around individual tanycyte cell bodies in infrared and/or fluorescent images. Changes in GCaMP3 fluorescence intensity were measured by plotting the intensity of ROI (minus background) over time, initial resting state fluorescence (F_0) was computed before drug application and subsequent fluorescence values ($F-F_0=\Delta F$) normalized to this ($\Delta F/F_0$). Drugs were puffed from a borosilicate-glass patch pipette (World Precision Instruments) pulled on a P1000 puller (Sutter Instrument Co). The pipette tip was positioned 25 μm from tanycyte cell bodies. Puffs were delivered against the direction of flow of perfusion at 4psi pressure using a PV820 pneumatic PicoPump (World Precision Instruments). Leptin and ATP (Sigma) concentrations in the patch pipette were 6 μM and 10mM (both in ACSF), respectively. To exclude mechanical responses of tanycytes to the puff, patch pipettes were also filled with ACSF alone.

Leptin receptor detection—Twelve-week-old C57Bl/6J mice were anesthetized with ketamine+xylazine and injected with the human anti mouse LepR monoclonal XPA antibody²⁶ (2nmol/animal, #XPA.80.037, XOMA Corporation, Berkeley, California, USA) into the jugular vein. As soon as the injection ended, mice were perfused with saline and 4% paraformaldehyde. 20 μm -thick cryostat sections were collected from cryoprotected brains and processed to reveal XPA using a 1h incubation at room temperature with Biotinylated Goat anti-human IgG (1:1000; Jackson ImmunoResearch Labs Cat#109-065-003, RRID:AB_2337621), VECTASTAIN® Elite ABC peroxidase kit (PK-6100, Vector Laboratories) and TSA Biotin Tyramide kit (SAT70001EA, Perkin Elmer) associated with Streptavidin AlexaFluor-568 (1:600; Thermo Fisher Scientific Cat#S-11226, RRID:AB_2315774).

Proximity ligation assay—Sections from fresh-frozen brains were fixed in 4% paraformaldehyde for 15 min, permeabilized and blocked with TritonX-100 (0.3%) and 5% Horse Serum/PBS for 1 h. Sections were incubated with XPA (Xoma Laboratories) and rabbit anti-EGFR (Sigma, Ab-1070) at 4 °C overnight. PLA was performed using a Duolink® In Situ Red Starter Kit Goat/Rabbit (Sigma-Aldrich) according to manufacturer's instructions. To assess signal specificity, only one primary antibody was used.

RNAscope fluorescent in situ hybridization (FISH)—FISH was performed either on 2% paraformaldehyde-perfused brain sections (*Egfr*) or fresh-frozen brain sections (*LepR*) of the ME of adult male mice using the RNAscope® Multiplex Fluorescent Kit v2 according to manufacturer's instructions (Advanced Cell Diagnostics, Inc., Newark, CA, USA). Specific probes were used to detect *LepR* variant 1 (471171, NM_146146.2, target region 3220-4109), *LepR* variant 3 (496901-C3, NM_001122899.1, target region 3291-4713), and *Egfr* (443551-C2, NM_207655.2, target region 58-2111) mRNAs.

Hybridization with a probe against the *B.subtilis* *dapB* gene (320871) was used as a negative control. Following *Egfr* FISH, vimentin immunolabeling was performed using chicken anti-Vimentin (1:500 Millipore Cat#AB1620, RRID:AB_90774) and AlexaFluor-647-conjugated goat anti-chicken antibodies (1:500; ThermoFisher Cat#A-21449, RRID:AB_2535). For FISH and vimentin immunofluorescence, image acquisition was performed using an inverted confocal microscope (LSM 710, Zeiss, Jena, Germany). AlexaFluor-488-and AlexaFluor-568-secondary antibodies and TSA plus Fluorescein, Cyanine-3 and Cyanine-5 were imaged at 493/562 nm, 568/643 and 640/740. UV laser (355nm) was used to image Hoechst and DAPI. Z-stack images were acquired with a W Plan-APOCHROMAT 20x objective (NA 0.5, zoom 1.0). High-magnification photomicrographs were acquired with a 63x objective (NA 1.4) using the Airyscan detector (Zeiss). Images for figures were pseudocolored, adjusted for brightness and contrast and merged using Photoshop (CC2019, Adobe Systems, San Jose, CA).

pSTAT3 immunohistochemistry and analysis—Adult mice were sacrificed by decapitation at lights-on. 20 μ m-thick coronal sections from fresh-frozen brains were postfixed in 2% paraformaldehyde during 1h and processed for immunofluorescence as described (Bouret et al., 2012) using rabbit anti-pSTAT3 (Tyr705) (1:1000; Cell Signaling Technology Cat#9131, RRID:AB_331586) primary and AlexaFluor-647-conjugated goat anti-rabbit secondary antibodies (1/500; Molecular Probes Cat#A-21244, RRID:AB_141663). Images were acquired using an AxioImager.Z2 Apotome microscope (AxioCam MRm camera, Zeiss). Slides were then coded to conceal treatment groups, and pSTAT3-immunoreactive cells counted in eight sections/animal.

Pancreatic islet studies—Pancreata were digested with type V collagenase (C9263; 1,5 mg/ml) for 11 min at 37°C as described (Annicotte et al., 2009, Rabhi et al., 2016), and separated on a density gradient, islets were handpicked under a dissection microscope and cultured overnight in RPMI-1640 (Gibco, 61870-010) containing 1mM FBS (Gibco, 10270-106) and Penicillin/streptomycin. For insulin secretion tests, ~30 islets were exposed to 2.8 mM or 20 mM glucose in Krebs-Ringer-bicarbonate HEPES buffer containing 0.5% fatty-acid-free BSA. Secreted insulin was measured 1h later using the Ultrasensitive Insulin ELISA kit (Merckodia). Data are expressed relative to total insulin content.

RNA extraction, measurements and profiling of pancreatic islets—Total RNA was extracted from islets using RNeasy Plus Micro Kit (Qiagen, Tokyo, Japan) following manufacturer's recommendations. mRNA levels were measured after reverse transcription by RT-qPCR with FastStart SYBR Green master mix (Roche) following manufacturer's recommendations and gene-specific oligonucleotides (Table S2). Expression levels were normalized to cyclophilin mRNA, and expressed using the formula 2^{-Ct} .

Immunofluorescence (IF) on pancreatic sections—IF was performed as described previously^{82,83}. Briefly, after antigen retrieval using citrate buffer (Sigma), 5 μ m-thick formalin-fixed pancreatic sections were incubated with anti-insulin (1:1000, Agilent Cat#A0564, RRID:AB_10013624) or anti-glucagon primary antibodies (1:1000, Sigma-Aldrich Cat#G2654, RRID:AB_259852) and AlexaFluor-594-conjugated goat anti guinea-

pig (1:500, Molecular Probes Cat#A-11076, RRID:AB_141930) and AlexaFluor-488-conjugated goat anti-mouse antibodies (1:500, Thermo Fisher Scientific Cat#A-11001, RRID:AB_2534069). Images were processed for morphometry using ImageJ software by an observer blind to experimental groups.

Western blot analyses of liver and WAT—Tissues were homogenized using a TissueLyser II (Qiagen, Tokyo, Japan) in cold RIPA buffer (containing 200mM Tris/HCl (pH 7.4), 130 mM NaCl, 10%(v/v) glycerol, 0.1%(v/v) SDS, 1%(v/v) TritonX-100, 10mM MgCl₂) with anti-proteases and anti-phosphatases (Sigma-Aldrich; St.Louis, MO), and lysates centrifuged for 30 min at 18000g at 4°C. Liver and White Adipose Tissue (WAT) total protein lysates were separated on SDS-polyacrylamide gels (SDS-PAGE), electrotransferred to PVDF membranes and probed successively with the following antibodies: hormone-sensitive lipase(HSL): (111000, Abcam Cat#ab45422, RRID:AB_2135367); phospho-HSL(Ser660): (111000, Cell Signaling Technology Cat#4126, RRID:AB_490997); Acetyl-CoA-Carboxylase 1 (Acc): (111000, Millipore Cat#04-322, RRID:AB_673047); phospho-Acc(Ser79): (111000, Cell Signaling Technology Cat#3661, RRID:AB_330337); lipoprotein lipase (111000, H-53; Santa Cruz Biotechnology Cat#sc-32885, RRID:AB_2234585); fatty acid synthase antibody (FAS): (115000, Abcam Cat#ab128870, RRID:AB_11143436); β -actin: (115000, Sigma-Aldrich Cat#A2228, RRID:AB_47669), after incubating membranes with 5% BSA blocking buffer. Proteins were detected using horseradish-peroxidase-conjugated secondary antibodies (#PI-2000; RRID:AB_2336177, Dako, Glostrup, Denmark). Specific immunolabeling was visualized using chemiluminescence following manufacturer's instructions (Pierce ECL Western Blotting Substrate, ThermoScientific, USA), and values expressed relative to β -actin.

Blood lipid determination—Serum cholesterol (1001093, Spinreact), triglycerides (1001310, Spinreact) and free fatty-acids levels (436-91995, 434-91795, WAKO) were measured on a ThermoScientific Multiskan GO spectrophotometer.

WAT histomorphology—WAT samples were fixed in 10% formalin for 24h, dehydrated and paraffin embedded. 3 μ m-thick sections were cut on a microtome, stained using standard alcoholic hematoxylin/eosin (BioOptica, Italy) and observed and photographed using a Provis AX70 microscope (Olympus, Corp, Tokyo, Japan). Digital images were quantified with ImageJ Software (NIH; USA).

Liver triglyceride content—Livers (~500mg) were homogenized for 3min in ice-cold chloroform-methanol (2:1, vol/vol). Triglycerides were extracted during 3h shaking at room temperature. For phase separation, mili-Q water was added, samples centrifuged and the organic bottom layer recollected. The organic solvent was dried using a Speed-Vac and the pellet redissolved in chloroform, and triglyceride content measured after solvent evaporation (1001310, Spinreact) by spectrophotometry on a ThermoScientific Multiskan GO spectrophotometer.

Oil red O Staining—Frozen 8 μ m sections of liver were cut with a cryostat and stained in filtered Oil red O for 10min. Sections were washed in distilled water, counterstained with

Mayer's hematoxylin for 3min, and mounted in aqueous mountant. Sections were observed and photographed using a Provis AX70 microscope (Olympus, Corp, Tokyo, Japan).

Primary culture and cell line experiments

Primary tanycyte culture—Tanycytes were isolated from the median eminence of the hypothalamus of 10-d-old rats and cultured as described previously^{54,84}. Briefly, after decapitation and removal of the brain, median eminences were dissected and crushed on 80µM nylon mesh (Sefar America Inc., Kansas City, MO). Dissociated cells were cultured in DMEM/F12 (Invitrogen, Cergy Pontoise, France) supplemented with 10% (v/v) donor calf serum (Invitrogen) under humid atmosphere of 5 % CO₂-95 % air at 37 °C. Culture medium was changed after 3-4 days of culture and subsequently every 2 days. Upon reaching confluence, the tanycytes were isolated from contaminating cells by overnight shaking at 250 rpm at 37 °C and either replated in 6 cm dishes for Western blot experiments or seeded in culture plates on poly-L-lysine-coated glass coverslips for studying leptin trafficking. Two days before treatment, the medium was replaced by a tanycyte defined medium (TDM) consisting of DMEM/F12 (devoid of phenol red; Invitrogen) supplemented with insulin (5µg/ml) (Sigma, Saint Quentin Fallavier, France) and putrescin (100µM) (Sigma).

PamGene arrays—Primary tanycyte cultures were incubated at 37°C with leptin (125nM) or DMSO for 2 or 15min before washing and snap-freezing. For kinome analysis, sample incubation, detection and analysis were performed on a PamStation 12 following manufacturer's instructions as previously described (Rabhi et al., 2018) using STK PamChip microarrays (PamGene International BV). Upstream kinases were identified using the Human Protein Reference Database (<http://www.hprd.org/>).

Fluorescent leptin internalization assay and immunofluorescence in primary cultures—Tanycytes were seeded on poly-L-lysine-coated glass coverslips (10µg/ml) and incubated in TDM (DMEM/F-12, #11039, ThermoFisher), 1% L-glutamine (#25030-024, ThermoFisher), 2% penicillinstreptomycin (#P4458, Sigma), insulin (111000, #I5500, Sigma), putrescine (11500, #P5780, Sigma) for 24h before the experiment. Tanycytes were incubated for the indicated time at 37°C with either bioactive fluorescent leptin (Fluorescent-leptin, 125nM, Cisbio Bioassays) or a fluorescent leptin antagonist (LAN, 125nM, Cisbio Bioassays), both diluted in TDM. Cells were then fixed for 10min at 4°C with 4% paraformaldehyde and washed thrice with PBS 1X. For cointernalization, tanycytes were incubated with Fluorescent-leptin and XPA (30nM in TDM, Xoma Laboratories) for 5min, washed and fixed. Cells were then washed and permeabilized with 0.1% TritonX-100 (v/v in PBS) for 5min at room temperature. All antibodies were diluted in PBS-3% BSA and incubated for 45min at room temperature: anti-EEA1 (11200; Santa Cruz Biotechnology Cat#sc-641 5, RRID:AB_2096822) followed by AlexaFluor-488-conjugated anti-goat (1/1000; Molecular Probes Cat#A-11055, RRID:AB_2534102) or AlexaFluor-488-conjugated anti-human antibodies (1/1000; Molecular Probes Cat#A-11013, RRID:AB_141360) to label XPA.

Fluorescent leptin release assay in primary culture—Tanycytes were incubated for 15min at 37°C with either Fluorescent-leptin (125 nM, Cisbio Bioassays) or LAN (125

nM; Cisbio Bioassays), washed and incubated with TDM for the indicated amount of time and fixed for 10min at 4°C with 4% PFA. To assess the role of MAPK pathway, tanycytes were preincubated for 30min with the MAPK inhibitor UO126 (10 μ M in TDM; #9903; Cell Signaling Technology), and Fluorescent-leptin uptake and release measured. To check for LAN release with EGF, EGF-TRITC (10 ng/ml; #3481; Molecular Probes) was added during the chase.

ELISA—To quantify leptin release, tanycytes were cultivated in 10cm Petri dishes, incubated with recombinant leptin (62.5nM, Protein Rehovot Laboratory) diluted in TDM for 15min at 37°C, and washed and incubated with TDM to chase leptin for the indicated amount of time. Leptin released into medium or retained in cells was quantified by ELISA following manufacturer's instructions (#MOB00; R&D Systems). Leptin secretion was expressed as a percentage of total leptin.

Image acquisition and analysis—Cells were observed under a TCS SP5 confocal microscope (Leica microsystems) and images were acquired according to Nyquist parameters using a 63x (NA 1.4) oil-immersion objective. Single-plane images were analyzed using open-source Icy software (<http://icy.bioimageanalysis.org/>). The cell periphery was manually delineated on phase-contrast images and object-based segmentation using wavelet transform algorithms (spot detector plugin) performed to detect vesicles in each channel. Objects were considered colocalized if their centroids were ≥ 3 pixels apart. EEA1 segmentation was used to estimate leptin in EEA1 compartments and calculated as a percentage of total leptin in cells.

Cell lines—HEK293T (ECACC Cat# 12022001, RRID:CVCL_0063), HeLa (ATCC Cat# CCL-2, RRID:CVCL_0030), CHO-mouse LepRb (gift from Xoma Corp laboratory), CHO (ATCC Cat# CCL-61, RRID:CVCL_0214) and N46 (from Dr. Belsham's lab, described in ⁸⁵) cells were grown in DMEM (Gibco, Life Technologies) with 4500mg/l glucose and 10% fetal calf serum (Invitrogen) in a 10% CO₂ humidified atmosphere at 37°C. HEK293T cells were transiently transfected (48h) with jetPEI (Polyplus-transfection), with a mock or LepR- or EGFR-expressing pCDNA3 plasmids, or LIFR- or IL6R-expressing pMET7 plasmids. The ERK signaling pathway was studied in transfected HEK29T cells expressing exogenous EGFR, LepRb or both receptors, with or without a 1h pretreatment with 1 μ M AG1478 inhibitor (T4182, Sigma) prior to 15min of stimulation with EGF (1nM), leptin (10nM) or both.

Western blotting on primary cultures and cell lines—The sequences and protocols to prepare extracellular sub-domains of LepR have been described previously ⁸⁶. Cell lysates (in Laemmli buffer with 30mM DTT, 2mM orthovanadate and 10mM NaF) were separated by SDS/PAGE, transferred to nitrocellulose membranes and immunoblotted with the following antibodies: anti-phospho-tyrosine (Tyr-705)-STAT3 (Cell Signaling Technology Cat#9145, RRID:AB_2491009), anti-STAT3 (Cell Signaling Technology Cat#9139, RRID:AB_331757), anti-phospho-tyrosine (Tyr-204)-ERK1/2 (Santa Cruz Biotechnology Cat#sc-1 6982, RRID:AB_2139990), anti-ERK2 (Proteintech Cat#51068-1-AP, RRID:AB_2250380), anti-FLAG tag (Sigma-Aldrich Cat#SAB4301135,

RRID:AB_2811010), anti-HA tag (Cell Signaling Technology Cat#3724) or XPA (Xoma Laboratories). Western blots were scanned on an Odyssey infrared Imaging System (Licor).

Co-Immunoprecipitation—HEK293T cells were transfected with a Flag-EGFR-expressing vector either with LepR-YFP or empty vector. 48h later, cells were harvested in lysis buffer containing Tris-EDTA-magnesium-1% TritonX-100 and solubilized for 2h (4°C, under rotation), centrifuged (14,000g, 45min), and supernatants subjected to immunoprecipitation with 2µg of anti-GFP antibody (Roche) for 4h, 4°C, under rotation. Protein G beads (Sigma-Aldrich) were then added, and after a 2h incubation, samples were washed in 0.1% TritonX-100 buffer by repeated centrifugation (1,000g, 5min). The pellet was resuspended in Laemmli buffer (62.5mM Tris/HCl pH6.8, 5% SDS, 10% glycerol, 0.005% bromophenol blue), heat-denatured (95°C, 5min), and separated by SDS-PAGE.

Bioluminescence resonance energy transfer (BRET)-based LepR biosensing

—HEK293T cells were transiently co-transfected in 12-well plates with 40ng of LepR-Luciferase plasmid and increasing amounts of LepR-YFP plasmids. Cells were grown overnight and transferred to 96-well Optiplates (PerkinElmer Life Sciences) pre-coated with 10µg/mL poly-L-lysine (Sigma), and grown for an additional 24h. The next day, cells were stimulated with leptin, XPA or vehicle for 30min at 37°C. After washing with PBS, Coelenterazine (Interchim France), a Luciferase substrate, was added to cells and emissions at Luciferase and YFP wavelength measured on a Tecan F500 plate-reader (Tecan; Männedorf, Switzerland).

TR-FRET binding assay—TR-FRET assays are based on energy transfer between a fluorescently-labeled donor (Terbium cryptate (Tb)) and a fluorescently-labeled acceptor (d2). In order to covalently label cell-surface EGFR or LepR, with Tb, the receptor is fused to the SNAP enzyme that can be covalently labeled with the Tb fluorophore at a stoichiometry of 1Tb per 1SNAP-receptor, using a suicide enzyme substrate-Tb. 48h post-transfection, HEK293T cells, expressing SNAP-EGFR+LepR or SNAP-LepR+EGFR, and previously plated in poly-L-lysine-coated 96-well plates were incubated with 100nM Tb-SNAP substrate in Tag-lite labeling medium (Cisbio Bioassays; 1h, 4°C). After several washes, cells were treated with different concentrations of leptin-d2 or EGF-d2 (CisbioAssays) respectively. For each concentration, non-specific binding was determined by adding an excess of unlabeled leptin or unlabeled EGF (200-500nM). The B_{max} signal and equilibrium dissociation constant (K_D) were obtained by fitting specific-binding data points (triplicate) with one-binding site model using GraphPad Prism software (GraphPad Software, Inc., San Diego, CA).

Statistics

Results are given as means±standard error of the mean (SEM). Samples or animals were excluded when their values were outside ±2SD, or when an objective experimental failure was observed; studies were not formally randomized and investigators were not blind to treatment group except when mentioned. To test if the populations followed a Gaussian distribution, a normality test was performed (Kolmogorov-Smirnov test for n between 5-7; Shapiro-Wilk test for $n > 7$). For normal distributions, twosided unpaired t-tests were

used to compare two populations⁸⁷⁻⁸⁹⁸⁶⁻⁸⁸⁸⁶⁻⁸⁸⁸⁵⁻⁸⁷⁸⁴⁻⁸⁶; for multiple-comparison tests, a one-way or two-way ANOVA followed by Tukey's *post hoc* multiple-comparison test was used (unless otherwise indicated in the figure legends). For non-Gaussian distributions, Mann-Whitney tests were used to compare two populations, and Kruskal-Wallis followed by Dunn's *post-hoc* test for multiple comparisons. Data analysis was performed using GraphPad Prism Software Version 7 (GraphPad, San Diego, CA). The threshold for significance was $p < 0.05$.

Supplementary Material

Refer to Web version on PubMed Central for supplementary material.

Acknowledgements

This work was supported by the Agence National de la Recherche (ANR-15-CE14-0025 to VP, RJ and SG and ANR-17-CE14-0034 to JSA), the European Research Council (ERC Synergy Grant WATCH No 810331 to VP, RN and MS), the National Institute of Health (NIH grant R01DK123002 to Y-BK and VP), « European Genomic Institute for Diabetes » (E.G.I.D, ANR-10-LABX-0046 to JSA and VP), DISTALZ (ANR-11-LABX-0009 to VP), I-SITE ULNE (ANR-16-IDEX-0004), the “Who am I?” (ANR-11-LABX-0071 to JD), the DHU Autoimmune and Hormonal Diseases (Authors) (JD), European Foundation for the Study of Diabetes (EFSD, to JSA), the Université de Lille (to MD, CB and JSA), Fondation pour la Recherche Médicale (FRM, to MD) and the H2020-MSCA-IF-2016 grant GLUCOTANYCYTES No 748134 to MI. We thank Laure Rolland for excellent technical help with immunofluorescence analysis of pancreatic sections and Raphaël Boutry and the UMR 8199 LIGAN-PM Genomic platform (ANR-10-EQPX-07-01) belonging to EGID for Kinome assays. We thank the UMS2014-US41 for technical support.

Data availability

The Human Protein Reference Database (<http://www.hprd.org>) was used to identify upstream kinases in the PamGene assay. Uncropped Western blots and Source Data Files for PamGene analyses are provided as Extended data. Additional data that support the findings of this study are available from the corresponding author upon request.

References

1. Swinburn BA, et al. The Global Syndemic of Obesity, Undernutrition, and Climate Change: The Lancet Commission report. *Lancet*. 2019; 393 :791–846. [PubMed: 30700377]
2. Yoon KH, et al. Epidemic obesity and type 2 diabetes in Asia. *Lancet*. 2006; 368 :1681–1688. [PubMed: 17098087]
3. Ohn JH, et al. 10-year trajectory of beta-cell function and insulin sensitivity in the development of type 2 diabetes: a community-based prospective cohort study. *Lancet Diabetes Endocrinol*. 2016; 4 :27–34. [PubMed: 26577716]
4. Ahima RS, Flier JS. Leptin. *Annu Rev Physiol*. 2000; 62 :413–437. [PubMed: 10845097]
5. de Luca C, et al. Complete rescue of obesity, diabetes, and infertility in db/db mice by neuron-specific LEPR-B transgenes. *J Clin Invest*. 2005; 115 :3484–3493. [PubMed: 16284652]
6. Cohen P, et al. Selective deletion of leptin receptor in neurons leads to obesity. *J Clin Invest*. 2001; 108 :1113–1121. [PubMed: 11602618]
7. Caron A, Lee S, Elmquist JK, Gautron L. Leptin and brain-adipose crosstalks. *Nat Rev Neurosci*. 2018; 19 :153–165. [PubMed: 29449715]
8. Pan WW, Myers MG Jr. Leptin and the maintenance of elevated body weight. *Nat Rev Neurosci*. 2018; 19 :95–105. [PubMed: 29321684]
9. Friedman JM. Leptin and the endocrine control of energy balance. *Nature Metabolism*. 2019; 1 :754–764.

10. Kamohara S, Burcelin R, Halaas JL, Friedman JM, Charron MJ. Acute stimulation of glucose metabolism in mice by leptin treatment. *Nature*. 1997; 389 :374–377. [PubMed: 9311777]
11. Coppari R, et al. The hypothalamic arcuate nucleus: a key site for mediating leptin's effects on glucose homeostasis and locomotor activity. *Cell Metab*. 2005; 1 :63–72. [PubMed: 16054045]
12. Buettner C, et al. Critical role of STAT3 in leptin's metabolic actions. *Cell Metab*. 2006; 4 :49–60. [PubMed: 16814732]
13. Buettner C, et al. Leptin controls adipose tissue lipogenesis via central, STAT3-independent mechanisms. *Nat Med*. 2008; 14 :667–675. [PubMed: 18516053]
14. Prevot V, et al. The Versatile Tanycyte: A Hypothalamic Integrator of Reproduction and Energy Metabolism. *Endocr Rev*. 2018; 39 :333–368. [PubMed: 29351662]
15. Garcia-Caceres C, et al. Role of astrocytes, microglia, and tanycytes in brain control of systemic metabolism. *Nat Neurosci*. 2019; 22 :7–14. [PubMed: 30531847]
16. Banks WA. The blood-brain barrier as an endocrine tissue. *Nat Rev Endocrinol*. 2019; 15 :444–455. [PubMed: 31127254]
17. Schaeffer M, et al. Rapid sensing of circulating ghrelin by hypothalamic appetite-modifying neurons. *Proc Natl Acad Sci U S A*. 2013; 110 :1512–1517. [PubMed: 23297228]
18. Ciofi P, et al. Brain-endocrine interactions: a microvascular route in the mediobasal hypothalamus. *Endocrinology*. 2009; 150 :5509–5519. [PubMed: 19837874]
19. Yulyaningsih E, et al. Acute Lesioning and Rapid Repair of Hypothalamic Neurons outside the Blood-Brain Barrier. *Cell Rep*. 2017; 19 :2257–2271. [PubMed: 28614713]
20. Djogo T, et al. Adult NG2-Glia Are Required for Median Eminence-Mediated Leptin Sensing and Body Weight Control. *Cell Metab*. 2016; 23 :797–810. [PubMed: 27166944]
21. Mullier A, Bouret SG, Prevot V, Dehouck B. Differential distribution of tight junction proteins suggests a role for tanycytes in blood-hypothalamus barrier regulation in the adult mouse brain. *J Comp Neurol*. 2010; 518 :943–962. [PubMed: 20127760]
22. Langlet F, et al. Tanycytic VEGF-A Boosts Blood-Hypothalamus Barrier Plasticity and Access of Metabolic Signals to the Arcuate Nucleus in Response to Fasting. *Cell Metab*. 2013; 17 :607–617. [PubMed: 23562080]
23. Balland E, et al. Hypothalamic tanycytes are an ERK-gated conduit for leptin into the brain. *Cell Metab*. 2014; 19 :293–301. [PubMed: 24506870]
24. Yuan X, Caron A, Wu H, Gautron L. Leptin Receptor Expression in Mouse Intracranial Perivascular Cells. *Front Neuroanat*. 2018; 12 :4. [PubMed: 29410615]
25. Yoo S, Cha D, Kim DW, Hoang TV, Blackshaw S. Tanycyte-Independent Control of Hypothalamic Leptin Signaling. *Front Neurosci*. 2019; 13 :240. [PubMed: 30941008]
26. Bhaskar V, et al. An allosteric antibody to the leptin receptor reduces body weight and reverses the diabetic phenotype in the Lep(ob)/Lep(ob) mouse. *Obesity (Silver Spring)*. 2016; 24 :1687–1694. [PubMed: 27330016]
27. Jo YH, Chen YJ, Chua SC Jr, Talmage DA, Role LW. Integration of endocannabinoid and leptin signaling in an appetite-related neural circuit. *Neuron*. 2005; 48 :1055–1066. [PubMed: 16364907]
28. Irani BG, Le Foll C, Dunn-Meynell A, Levin BE. Effects of leptin on rat ventromedial hypothalamic neurons. *Endocrinology*. 2008; 149 :5146–5154. [PubMed: 18556346]
29. Kusumakshi S, et al. A Binary Genetic Approach to Characterize TRPM5 Cells in Mice. *Chem Senses*. 2015; 40 :413–425. [PubMed: 25940069]
30. Niv-Spector L, et al. Identification of the hydrophobic strand in the A-B loop of leptin as major binding site III: implications for large-scale preparation of potent recombinant human and ovine leptin antagonists. *Biochem J*. 2005; 391 :221–230. [PubMed: 15952938]
31. Muller-Fielitz H, et al. Tanycytes control the hormonal output of the hypothalamic-pituitary-thyroid axis. *Nat Commun*. 2017; 8 :484 [PubMed: 28883467]
32. Frayling C, Britton R, Dale N. ATP-mediated glucosensing by hypothalamic tanycytes. *J Physiol*. 2011; 589 :2275–2286. [PubMed: 21486800]
33. Auriou J, et al. Gain of affinity for VEGF165 binding within the VEGFR2/NRP1 cellular complex detected by an HTRF-based binding assay. *Biochem Pharmacol*. 2018; 158 :45–59. [PubMed: 30236477]

34. Vauthier V, et al. Design and validation of a homogeneous time-resolved fluorescence-based leptin receptor binding assay. *Anal Biochem.* 2013; 436 :1–9. [PubMed: 2333588]
35. Langlet F, Mullier A, Bouret SG, Prevot V, Dehouck B. Tanycyte-like cells form a blood-cerebrospinal fluid barrier in the circumventricular organs of the mouse brain. *J Comp Neurol.* 2013; 521 :3389–3405. [PubMed: 23649873]
36. Howard JK, Flier JS. Attenuation of leptin and insulin signaling by SOCS proteins. *Trends Endocrinol Metab.* 2006; 17 :365–371. [PubMed: 17010638]
37. Chmielewski A, et al. Preclinical Assessment of Leptin Transport into the Cerebrospinal Fluid in Diet-Induced Obese Minipigs. *Obesity (Silver Spring).* 2019; 27 :950–956. [PubMed: 31006983]
38. Balland E, Chen W, Tiganis T, Cowley MA. Persistent leptin signalling in the arcuate nucleus impairs hypothalamic insulin signalling and glucose homeostasis in obese mice. *Neuroendocrinology.* 2019
39. Sukumaran S, Xue B, Jusko WJ, Dubois DC, Almon RR. Circadian variations in gene expression in rat abdominal adipose tissue and relationship to physiology. *Physiol Genomics.* 2010; 42A :141–152. [PubMed: 20682845]
40. Tschop M, Smiley DL, Heiman ML. Ghrelin induces adiposity in rodents. *Nature.* 2000; 407 :908–913. [PubMed: 11057670]
41. Schwartz MW, et al. Specificity of leptin action on elevated blood glucose levels and hypothalamic neuropeptide Y gene expression in ob/ob mice. *Diabetes.* 1996; 45 :531–535. [PubMed: 8603777]
42. Pelleymounter MA, et al. Effects of the obese gene product on body weight regulation in ob/ob mice. *Science.* 1995; 269 :540–543. [PubMed: 7624776]
43. Berglund ED, et al. Direct leptin action on POMC neurons regulates glucose homeostasis and hepatic insulin sensitivity in mice. *J Clin Invest.* 2012; 122 :1000–1009. [PubMed: 22326958]
44. Back SH, Kaufman RJ. Endoplasmic reticulum stress and type 2 diabetes. *Annu Rev Biochem.* 2012; 81 :767–793. [PubMed: 22443930]
45. Sohn JW, et al. Melanocortin 4 receptors reciprocally regulate sympathetic and parasympathetic preganglionic neurons. *Cell.* 2013; 152 :612–619. [PubMed: 23374353]
46. Muzumdar R, et al. Physiologic effect of leptin on insulin secretion is mediated mainly through central mechanisms. *FASEB J.* 2003; 17 :1130–1132. [PubMed: 12709405]
47. Fagerholm V, Haaparanta M, Scheinin M. alpha2-adrenoceptor regulation of blood glucose homeostasis. *Basic Clin Pharmacol Toxicol.* 2011; 108 :365–370. [PubMed: 21418144]
48. Rosengren AH, et al. Overexpression of alpha2A-adrenergic receptors contributes to type 2 diabetes. *Science.* 2010; 327 :217–220. [PubMed: 19965390]
49. Wang P, et al. A leptin-BDNF pathway regulating sympathetic innervation of adipose tissue. *Nature.* 2020; 583 :839–844. [PubMed: 32699414]
50. Ahima RS, et al. Role of leptin in the neuroendocrine response to fasting. *Nature.* 1996; 382 :250–252. [PubMed: 8717038]
51. Zhou Y, et al. Temporal dynamic reorganization of 3D chromatin architecture in hormone-induced breast cancer and endocrine resistance. *Nat Commun.* 2019; 10 1522 [PubMed: 30944316]
52. Liu Z, et al. Short-term tamoxifen treatment has long-term effects on metabolism in high-fat diet-fed mice with involvement of Nmnat2 in POMC neurons. *FEBS Lett.* 2018; 592 :3305–3316. [PubMed: 30192985]
53. Shida D, Kitayama J, Mori K, Watanabe T, Nagawa H. Transactivation of epidermal growth factor receptor is involved in leptin-induced activation of janus-activated kinase 2 and extracellular signal-regulated kinase 1/2 in human gastric cancer cells. *Cancer Res.* 2005; 65 :9159–9163. [PubMed: 16230373]
54. Prevot V, Cornea A, Mungenast A, Smiley G, Ojeda SR. Activation of erbB-1 signaling in tanycytes of the median eminence stimulates transforming growth factor beta1 release via prostaglandin E2 production and induces cell plasticity. *J Neurosci.* 2003; 23 :10622–10632. [PubMed: 14627647]
55. Lomniczi A, Cornea A, Costa ME, Ojeda SR. Hypothalamic tumor necrosis factor-alpha converting enzyme mediates excitatory amino acid-dependent neuron-to-glia signaling in the neuroendocrine brain. *J Neurosci.* 2006; 26 :51–62. [PubMed: 16399672]

56. Balthasar N, et al. Leptin receptor signaling in POMC neurons is required for normal body weight homeostasis. *Neuron*. 2004; 42 :983–991. [PubMed: 15207242]
57. van de Wall E, et al. Collective and individual functions of leptin receptor modulated neurons controlling metabolism and ingestion. *Endocrinology*. 2008; 149 :1773–1785. [PubMed: 18162515]
58. Vauthier V, et al. Endospalin1 affects oppositely body weight regulation and glucose homeostasis by differentially regulating central leptin signaling. *Mol Metab*. 2017; 6 :159–172. [PubMed: 28123946]
59. Obici S, et al. Central melanocortin receptors regulate insulin action. *J Clin Invest*. 2001; 108 :1079–1085. [PubMed: 11581309]
60. Fan W, et al. The central melanocortin system can directly regulate serum insulin levels. *Endocrinology*. 2000; 141 :3072–3079. [PubMed: 10965876]
61. Rossi J, et al. Melanocortin-4 receptors expressed by cholinergic neurons regulate energy balance and glucose homeostasis. *Cell Metab*. 2011; 13 :195–204. [PubMed: 21284986]
62. Coppari R, Bjorbaek C. Leptin revisited: its mechanism of action and potential for treating diabetes. *Nat Rev Drug Discov*. 2012; 11 :692–708. [PubMed: 22935803]
63. Colberg SR, Simoneau JA, Thaete FL, Kelley DE. Skeletal muscle utilization of free fatty acids in women with visceral obesity. *J Clin Invest*. 1995; 95 :1846–1853. [PubMed: 7706491]
64. Beaufrere B, Morio B. Fat and protein redistribution with aging: metabolic considerations. *Eur J Clin Nutr*. 2000; 54 (Suppl 3) :S48–53. [PubMed: 11041075]
65. Zamboni M, Mazzali G, Fantin F, Rossi A, Di Francesco V. Sarcopenic obesity: a new category of obesity in the elderly. *Nutr Metab Cardiovasc Dis*. 2008; 18 :388–395. [PubMed: 18395429]
66. Parr EB, Coffey VG, Hawley JA. ‘Sarcobesity’: a metabolic conundrum. *Maturitas*. 2013; 74 :109–113. [PubMed: 23201324]
67. Tian S, Xu Y. Association of sarcopenic obesity with the risk of all-cause mortality: A meta-analysis of prospective cohort studies. *Geriatr Gerontol Int*. 2016; 16 :155–166. [PubMed: 26271226]
68. Okun JG, Rusu PM, Chan AY, et al. Liver alanine catabolism promotes skeletal muscle atrophy and hyperglycaemia in type 2 diabetes. *Nat Metab*. 2021; 3 :394–409. [PubMed: 33758419]
69. Prentki M, Nolan CJ. Islet beta cell failure in type 2 diabetes. *J Clin Invest*. 2006; 116 :1802–1812. [PubMed: 16823478]
70. Steil GM, et al. Adaptation of beta-cell mass to substrate oversupply: enhanced function with normal gene expression. *Am J Physiol Endocrinol Metab*. 2001; 280 :E788–796. [PubMed: 11287362]
71. Tuomi T, et al. The many faces of diabetes: a disease with increasing heterogeneity. *Lancet*. 2014; 383 :1084–1094. [PubMed: 24315621]
72. Morimoto A, et al. Impact of impaired insulin secretion and insulin resistance on the incidence of type 2 diabetes mellitus in a Japanese population: the Saku study. *Diabetologia*. 2013; 56 :1671–1679. [PubMed: 23680915]
73. Cohen P, et al. Selective deletion of leptin receptor in neurons leads to obesity. *J Clin Invest*. 2001; 108 :1113–1121. [PubMed: 11602618]
74. Peitz M, Pfannkuche K, Rajewsky K, Edenhofer F. Ability of the hydrophobic FGF and basic TAT peptides to promote cellular uptake of recombinant Cre recombinase: a tool for efficient genetic engineering of mammalian genomes. *Proc Natl Acad Sci U S A*. 2002; 99 :4489–4494. [PubMed: 11904364]
75. Figueira C, et al. Hypothalamic dopamine signaling regulates brown fat thermogenesis. *Nat Metab*. 2019; 1 :811–829. [PubMed: 31579887]
76. Quinones M, et al. Sirt3 in POMC neurons controls energy balance in a sex-and diet-dependent manner. *Redox Biol*. 2021; 41 101945 [PubMed: 33744652]
77. Bruss MD, Khambatta CF, Ruby MA, Aggarwal I, Hellerstein MK. Calorie restriction increases fatty acid synthesis and whole body fat oxidation rates. *Am J Physiol Endocrinol Metab*. 2010; 298 :E108–116. [PubMed: 19887594]

78. Imbernon M, et al. Central melanin-concentrating hormone influences liver and adipose metabolism via specific hypothalamic nuclei and efferent autonomic/JNK1 pathways. *Gastroenterology*. 2013; 144 :636–649. e636 [PubMed: 23142626]
79. Nogueiras R, et al. The central melanocortin system directly controls peripheral lipid metabolism. *J Clin Invest*. 2007; 117 :3475–3488. [PubMed: 17885689]
80. Golde WT, Gollobin P, Rodriguez LL. A rapid, simple, and humane method for submandibular bleeding of mice using a lancet. *Lab Anim (NY)*. 2005; 34 :39–43.
81. Clasadonte J, Scemes E, Wang Z, Boison D, Haydon PG. Connexin 43-Mediated Astroglial Metabolic Networks Contribute to the Regulation of the Sleep-Wake Cycle. *Neuron*. 2017; 95 :1365–1380. e1365 [PubMed: 28867552]
82. Annicotte JS, et al. The CDK4-pRB-E2F1 pathway controls insulin secretion. *Nat Cell Biol*. 2009; 11 :1017–1023. [PubMed: 19597485]
83. Blanchet E, et al. E2F transcription factor-1 regulates oxidative metabolism. *Nat Cell Biol*. 2011; 13 :1146–1152. [PubMed: 21841792]
84. de Seranno S, et al. Role of estradiol in the dynamic control of tanycyte plasticity mediated by vascular endothelial cells in the median eminence. *Endocrinology*. 2010; 151 :1760–1772. [PubMed: 20133455]
85. Dhillon SS, Belsham DD. Leptin differentially regulates NPY secretion in hypothalamic cell lines through distinct intracellular signal transduction pathways. *Regul Pept*. 2011; 167 :192–200. [PubMed: 21262273]
86. Zabeau L, et al. Selection of non-competitive leptin antagonists using a random nanobody-based approach. *Biochem J*. 2012; 441 :425–434. [PubMed: 21851341]
87. Student. The probable error of a mean. *Biometrika*. 1908; 6 :1–25.
88. Fay DS, Gerow K. A biologist's guide to statistical thinking and analysis (). *WormBook : the online review of C. elegans biology*. 2013; doi: 10.1895/wormbook.1891.1159.1891
89. Charan J, Biswas T. How to Calculate Sample Size for Different Study Designs in Medical Research? *Indian Journal of Psychological Medicine*. 2013; 35 :121–126. [PubMed: 24049221]

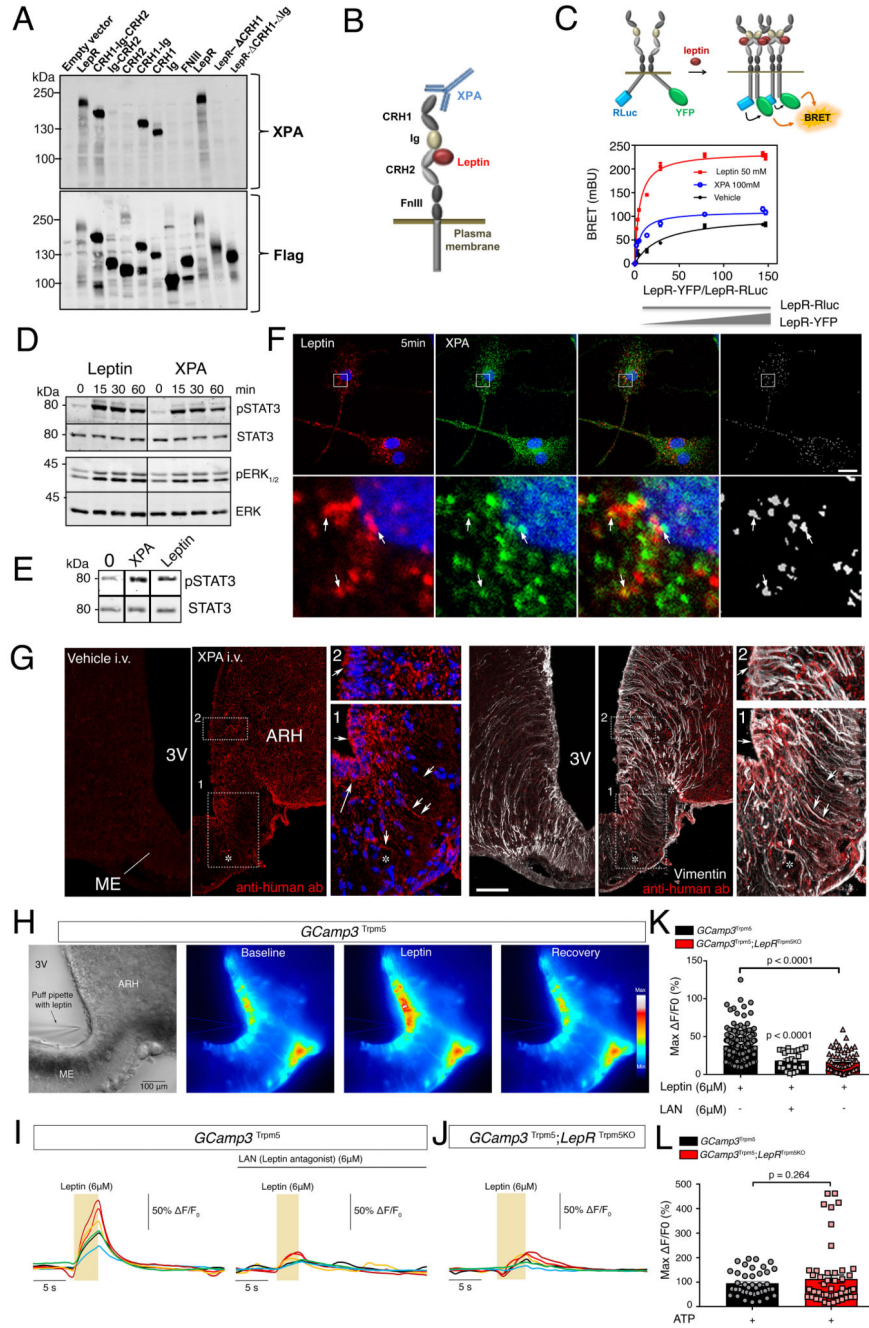


Figure 1. Tanyctes of the median eminence express functional leptin receptors
(A) Representative Western blot detection using the XPA antibody of different exogenously expressed LepR domains in HEK293 cells. Experiments were repeated at least twice.
(B) Schematic representation of leptin receptor domains and the XPA binding site.
(C) *Top*: schematic representation of the BRET assay to study the ligand-induced conformational change/interaction between LepR-Rluc and LepR-YFP. *Bottom*: BRET donor saturation curves in HEK293T cells with a constant expression level of LepR-Rluc

and increasing levels of LepR-YFP, upon stimulation with vehicle, leptin (50nM) or XPA (100nM) for 30 min at 37°C.

(D) STAT3 and ERK1/2 phosphorylation in HEK293 cells stably expressing LepR after stimulation with 50 nM leptin or 100 nM XPA for 5, 15, 30 or 60 minutes. Representative Western blot out of at least 2 independent experiments.

(E) STAT3 phosphorylation in tanycytes upon 50 nM leptin or 100 nM XPA stimulation for 30 minutes. Representative Western blot out of 2 independent primary cultures of tanycytes.

(F) Leptin colocalizes with LepR in primary tanycytes. Representative confocal images of tanycytes treated for 5 min with 125 nM fluorescent leptin (red) together with 33 nM XPA antibodies against LepR labeled with fluorescent secondary antibodies (green). The extent of colocalization is represented by the mask on the right. Arrows point to examples of colocalized pixels. Scale bar: 10 μ m. Experiments were repeated in 2 independent primary cultures of tanycytes.

(G) Representative photomicrograph revealing sites of XPA fixation in tanycytes of the median eminence (vimentin-positive cells) 2 minutes after intravenous XPA injection (2 nmol/animal) *in vivo* (n=3 mice per group). White arrows show XPA (red) and vimentin (white) colocalization. 3V: third ventricle; ARH: arcuate nucleus of the hypothalamus; ME: median eminence. Scale bar: 200 μ m.

(H) Representative image of a living brain slice containing the median eminence from a *GCamp3*^{Trpm5} mouse under bright-field and fluorescence microscopy, showing the reversible increase in intracellular calcium levels in tanycytic cell bodies lining the third ventricle (3V) upon the local application of a puff of leptin (6 μ M) via a glass pipette. The experiment was repeated in 5 mice. ME: median eminence. Scale bar: 100 μ m

(I) Representative curves of GCamp3 fluorescence (calcium current) over time (Δ T) compared to the baseline in tanycytes in living hypothalamic slices during a puff of leptin (yellow rectangle, 6 μ M), alone (left curve) or after pre-treatment with leptin antagonist (LAN, 6 μ M, top black line; right curve), in a *GCamp3*^{Trpm5} mouse.

(J) Same measurement as in **(I)** in a *GCamp3*^{Trpm5}; *LepR*^{Trpm5} mouse lacking LepR in tanycytes after a puff of leptin (6 μ M, yellow rectangle).

(K) Graph representing maximum difference in calcium concentration from baseline during the treatment of living brain slices in *GCamp3*^{Trpm5} and *GCamp3*^{Trpm5}; *LepR*^{Trpm5} mice, described in **(I)** and **(J)**. Kruskal Wallis with Dunn's; N=5 (*GCamp3*^{Trpm5} + leptin), 3 (*GCamp3*^{Trpm5} + LAN and leptin) and 4 (*GCamp3*^{Trpm5}; *LepR*^{Trpm5}) mice; each dot represents one cell (n=146,28,58). Values indicate means \pm SEM.

(L) Graph representing maximum difference in calcium concentration from baseline during a puff of ATP (10 mM) in living brain slices from *GCamp3*^{Trpm5} and *GCamp3*^{Trpm5}; *LepR*^{Trpm5} mice. Mann-Whitney test; N=3 mice per condition; each dot represents one cell (n=40,53). Values indicate means \pm SEM. See also Supplementary Figure 1.

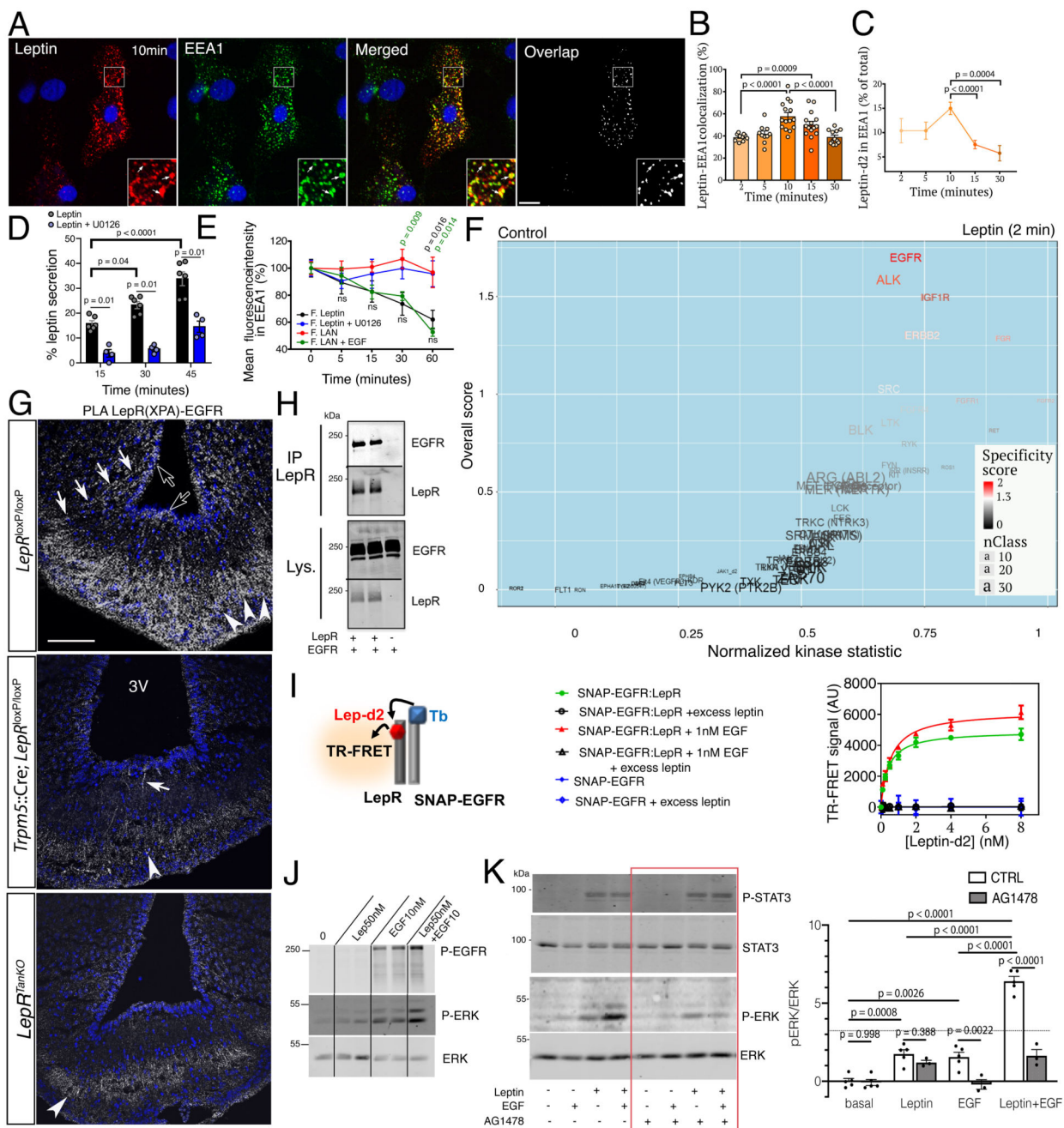


Figure 2. Tancytic EGFR physically interacts with LepR *in vivo* and plays a role in leptin transcytosis *in vitro*

(A) Endocytosed leptin colocalizing with early endosomes. Representative confocal images showing primary tanycytes treated for 10 min with 125 nM fluorescent leptin (red) and antibodies to the early endosome marker EEA1 (green). The extent of colocalization is represented by the mask on the right. Arrows in inset point to examples of colocalized pixels. Scale bar: 10µm.

- (B)** Percentage of leptin colocalizing with EEA1 over time following object-based detection of fluorescent leptin and EEA1 vesicles. Mann-Whitney test. n=10,10,15,15,12 cells as shown by individual dots from at least 2 independent primary cultures. Values represent means \pm SEM.
- (C)** Percentage of endocytosed leptin found in the EEA1-positive compartment over time. Mann-Whitney test. n=11,11,15,13,9 cells at 2,5,10,15 and 30 min, respectively, from at least 2 independent primary cultures. Values represent means \pm SEM.
- (D)** Leptin secreted into the medium by primary cultures of tanycytes as a percentage of total leptin concentration (intracellular and medium) 15, 30 and 45 minutes after fluorescent leptin addition. One-way ANOVA and Tukey's test. n=4 and 6 wells cells as shown by individual dots from at least 2 independent primary cultures. Values represent means \pm SEM.
- (E)** Percentage (as % of 0 min time point) of endocytosed fluorescent leptin or fluorescent LAN found in EEA1 compartments over time in cells treated or not with U0126 (leptin) or EGF (LAN). Mann-Whitney test. n=18,19,17,14,14 (leptin), 30,28,31,22,12 (LAN), 15,8,7,8,9 (Leptin+U0126) 15,13,14,13,10 (LAN+EGF) at 0,5,15,30,60 min, respectively, from at least 2 independent primary cultures. Values represent means \pm SEM.
- (F)** Volcano plot showing differences in peptide phosphorylation between primary cultures of tanycytes treated for 2 min with vehicle (PBS pH 8.0) or leptin (1 μ g/ml in PBS pH 8.0) (n=4 wells per condition). See also corresponding Source Data Files (Extended data Table 1 and 2).
- (G)** Proximity Ligation Assay (PLA) between LepR and EGFR using XPA and a rabbit anti-EGFR antibody. PLA signal is seen in tanycytic cell bodies (empty arrows), processes (white arrows) and end-feet in the external zone of the median eminence, where they contact the fenestrated endothelium of the pituitary portal circulation (arrowheads). Scale bar: 100 μ m.
- (H)** Co-immunoprecipitation of EGFR along with LepR in HEK293T cells; no co-immunoprecipitation of EGFR is observed when LepR is not expressed. IP, immunoprecipitation; Lys., cell lysate.
- (I)** Schematic representation of the TR-FRET technique (left). Right: specific saturation curves of leptin-d2 binding to its cognate receptor LepR within the LepR:SNAP-EGFR complex at the cell surface are obtained after 3h at 37°C. Data are presented as means \pm SD of 3 replicates of 1 representative experiment out of 3 independent experiments.
- (J)** Phosphorylation of EGFR and ERK upon addition of leptin 50nM, EGF 10nM or both for 30min at 37°C in primary tanycytes.
- (K)** Phosphorylation of STAT3 and ERK upon addition of leptin 10nM, EGF 1nM or both for 30min at 37°C in HEK293T cells expressing endogenous EGFR and transfected with LepRb in the presence or absence of the EGFR inhibitor AG1478 (1 μ M). Two-way ANOVA and Sidak's multiple comparison. n=5,5,3,5,3,5,3 wells as shown by individual dots from 2 independent experiments.

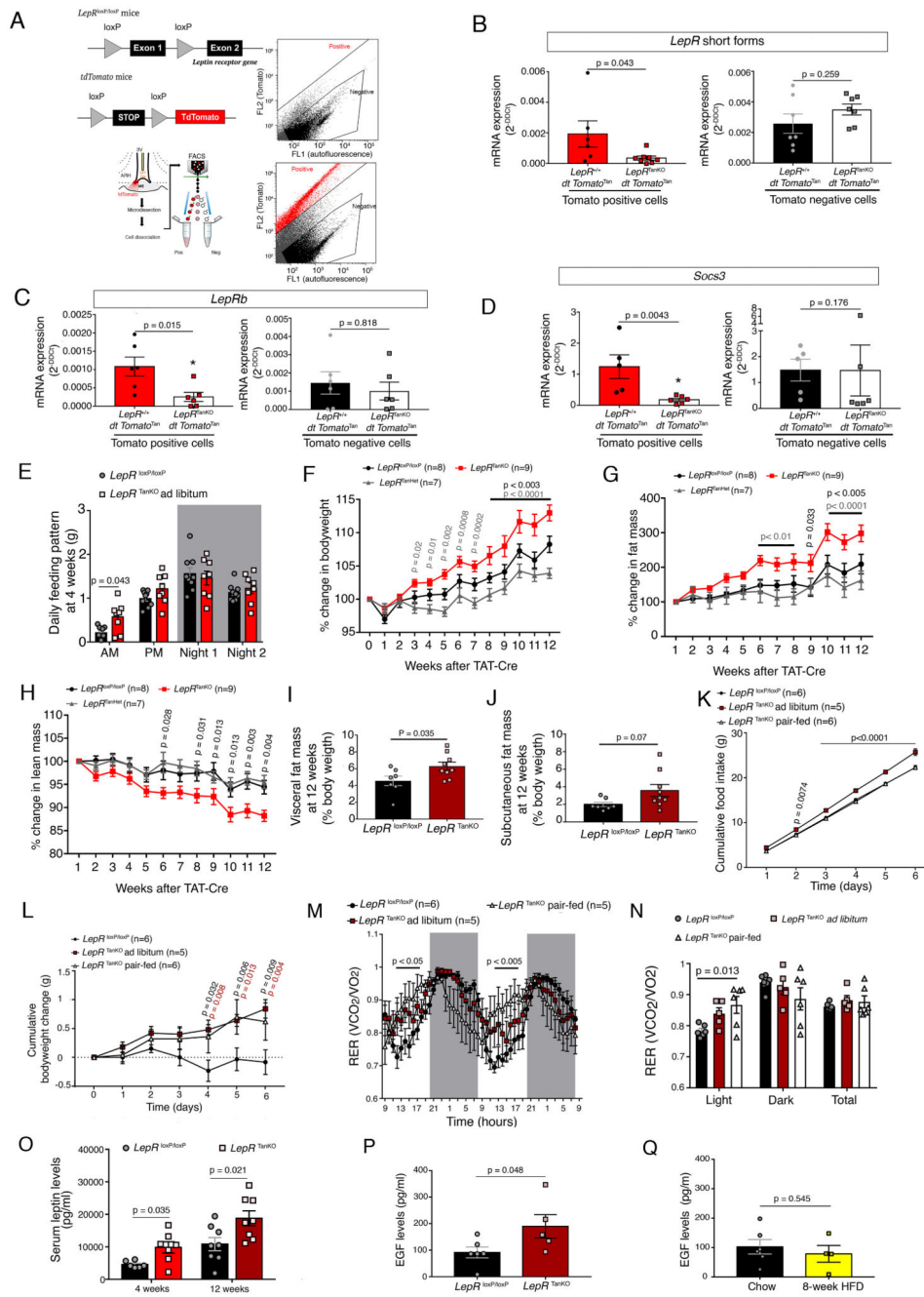


Figure 3. Selective LepR deletion in tanycytes causes food-intake-independent body weight gain and increased adiposity

(A) Schematic diagram and gating strategy for sorting Tomato positive cells following vehicle (top panel) and TAT-Cre infusion (bottom panel) into the third ventricle (3V) of *LepR^{+/+};tdTomato^{loxP-STOP-loxP}* or *LepR^{loxP/loxP};tdTomato^{loxP-STOP-loxP}* littermates. (B-D) mRNA expression levels of short forms (B) and the long form, LepRb (C), of the leptin receptor, and of Socs3 (D) in tdTomato-positive cells (left panels) and tdTomato-negative cells (right panels). A two-sided unpaired Student t-test or Mann-Whitney U test

was applied, depending on Shapiro-Wilk normality test results. Values indicate means \pm SEM. Each dot represents a mouse (n=6,8,7,7 in **B**, 6,6,6,6 in **C**, 5,6,5,6 in **D**).

(E) Food intake pattern (daily average of automatic measurements in metabolic cages over 24h), showing an increase at lights-on in $LepR^{TanKO}$ mice when compared to $LepR^{loxP/loxP}$ littermates. The night was divided in two 6h time slots (Night 1 and Night 2). Two-sided unpaired t-tests. Values indicate means \pm SEM. Each dot represents a mouse (n=10,8).

(F-H) Curves representing the kinetics of the % change in body weight (**F**), % change in fat mass (**G**) and % change in lean mass (**H**) between $LepR^{loxP/loxP}$, $LepR^{TanHet}$ and $LepR^{TanKO}$ through the 12 weeks following the TAT-Cre infusion into the 3V. Two-way ANOVA with Tukey's correction; Values represent means \pm SEM; n indicates the number of mice.

(I,J) Visceral fat mass (**I**) and subcutaneous (**J**) 12 weeks after TAT-Cre infusion. Mann-Whitney U test. Values indicate means \pm SEM. Each dot represents a mouse (n=7,9).

(K) Cumulative food intake in $LepR^{TanKO}$ pair-fed mice 12 weeks after TAT-Cre infusion compared to their control littermates. Two-way ANOVA with Tukey's correction. Values indicate means \pm SEM; n indicates the number of mice.

(L) Cumulative body weight change. Two-way ANOVA with Tukey's correction. Values indicate means \pm SEM; n indicates the number of mice.

(M) Energy ratio (RER) over time. Two-way ANOVA with uncorrelated Fisher's LSD test. Values indicate means \pm SEM; n indicates the number of mice.

(N) Mean energy ratio (RER) during light phase, dark phase and total. Two-way ANOVA with Tukey's correction. Values indicate means \pm SEM. Each dot represents a mouse (n=6,5,5).

(O) Circulating leptin levels in $LepR^{loxP/loxP}$ and $LepR^{TanKO}$ animals at 4 weeks and 12 weeks after TAT-Cre infusion into the 3V. Mann-Whitney test (4 weeks) and two-sided unpaired t-test (12 weeks). Values represent means \pm SEM. Each dot represents a mouse (n=6,7,8,8).

(P) Basal serum EGF concentrations in $LepR^{loxP/loxP}$ and $LepR^{TanKO}$ mice, 12 weeks after TAT-Cre infusion. Mann-Whitney U test. Values represent means \pm SEM. Each dot represents a mouse (n=6,5).

(Q) Basal serum EGF concentrations in C57Bl/6J mice fed normal chow or those fed a high-fat diet for 8 weeks. Mann-Whitney U test. Values represent means \pm SEM. Each dot represents a mouse (n=6,5).

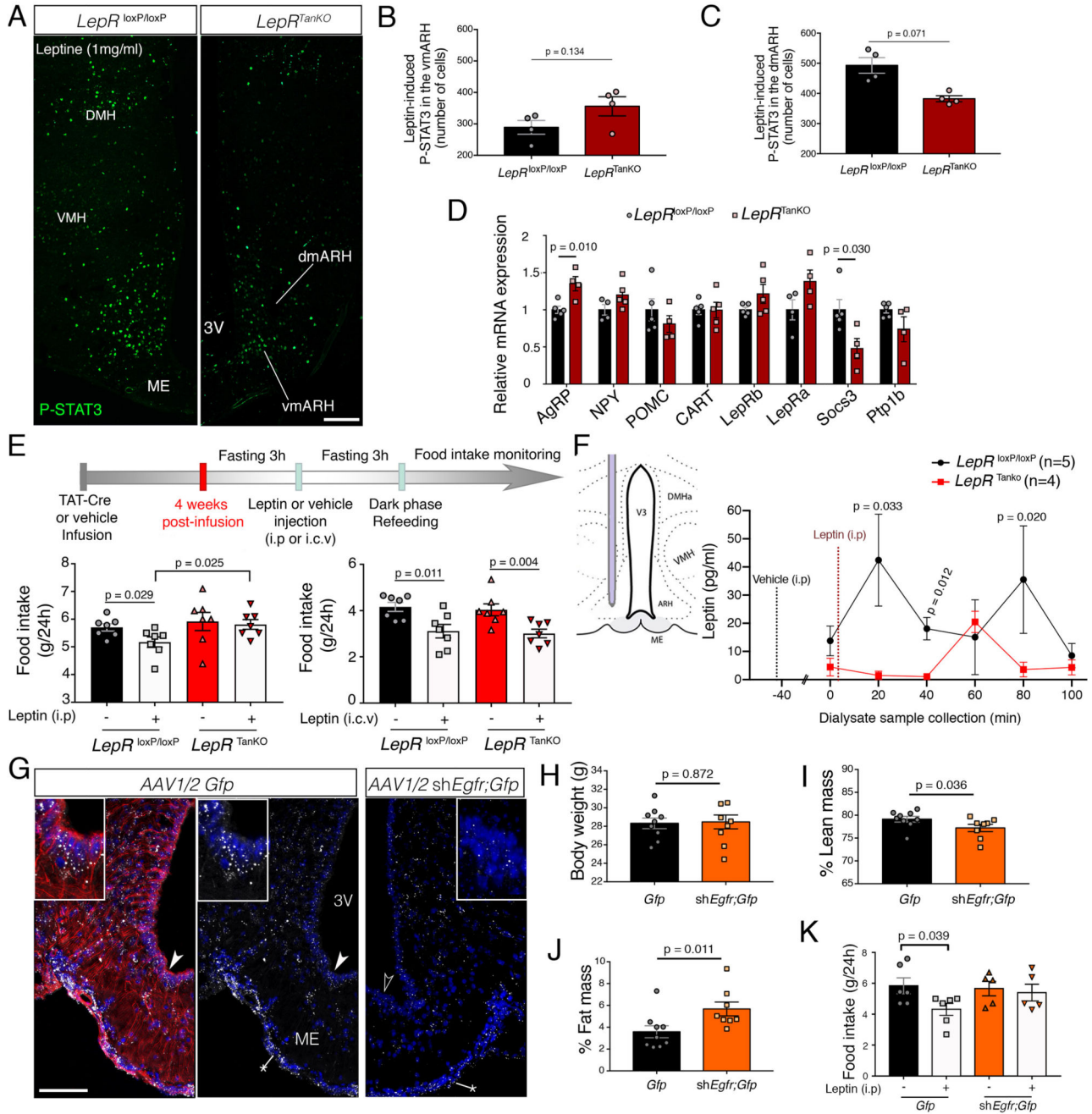


Figure 4. Defective LepR and EGFR signaling in tanycytes causes hypothalamic resistance to circulating leptin.

(A-C) Representative photomicrograph (A) and quantification of leptin-induced P-STAT3 immunofluorescence in the ventromedial (vm) (B) and dorsomedial (dm) arcuate nucleus (ARH) (C). Scale bar: 200µm. Two-sided unpaired Student’s t-test. Values indicate means ± SEM. Each dot represents a mouse (n=4,4).

(D) Relative mRNA expression levels of several genes known to be involved in the hypothalamic regulation of energy homeostasis and leptin activity in the microdissected

mediobasal hypothalamus (MBH) of *LepR^{loxP/loxP}* and *LepR^{TanKO}* mice, 12 weeks after TAT-Cre infusion. Student's t-test or Mann-Whitney U test, depending on Shapiro-Wilk normality test results. Values indicate means \pm SEM. Each dot represents a mouse (n=5,4).

(E) Schematic diagram showing the design of the experiment investigating the anorectic response to either intraperitoneal (i.p) or intracerebroventricular (i.c.v) leptin administration. Bottom left graph represents food intake in *LepR^{loxP/loxP}* (black and grey bars) and *LepR^{TanKO}* mice (red and pink bars) 24h after i.p. leptin (3mg/kg, grey and pink bars) or vehicle (PBS pH 8.0, black and red bars) administration. Bottom right graph represents food intake in *LepR^{loxP/loxP}* and *LepR^{TanKO}* mice 24h after i.c.v. leptin (2 μ g in 2 μ L) or vehicle (2 μ L PBS pH 8.0) injection. Mann-Whitney U test; Values indicate means \pm SEM. Each dot represents a mouse (n=7 per group).

(F) Leptin concentrations in the ARH interstitial liquid collected by microdialysis every 20 minutes following i.p. vehicle (t_{-40 min}) or leptin (t_{-1 min}) injection in *LepR^{loxP/loxP}* (n=7) and *LepR^{TanKO}* mice (n=6). Two-way ANOVA followed by Fisher's LSD post hoc test analysis was applied; Values indicate means \pm SEM; n indicates the number of mice.

(G) Representative photomicrograph of *in situ* hybridization of EGFR in the median eminence using RNAscope technology from mice injected with *AAV1/2 Dio2::gfp* or *AAV(1+2)-GFP-U6-m-EGFR-shRNA*. The experiment was performed in 3 animals per condition. The left panel shows vimentin-immunoreactivity in red. Arrowheads show the cells seen at higher magnification in insets. Scale bar: 100 μ m (25 μ m in inset).

(H-J) Curves representing the evolution of body weight (**H**), % change in fat mass (**I**) and % change in lean mass (**J**) between mice injected with *AAV1/2 Dio2::gfp* (control in black) or *AAV(1+2)-GFP-U6-m-EGFR-shRNA* (in orange) over 4 weeks following the beginning of the viral activity. Two-way ANOVA with Tukey's correction. Values indicate means \pm SEM; each dot represents a mouse (n=9,8).

(K) Graph representing food intake in mice injected with *AAV1/2 Dio2::gfp* or *AAV(1+2)-GFP-U6-m-EGFR-shRNA* 24h after i.p. leptin (1mg/kg) or vehicle (PBS pH 8.0) injection. An two-sided unpaired t-test was applied. Values indicate means \pm SEM; each dot represents a mouse (n=6 per group).

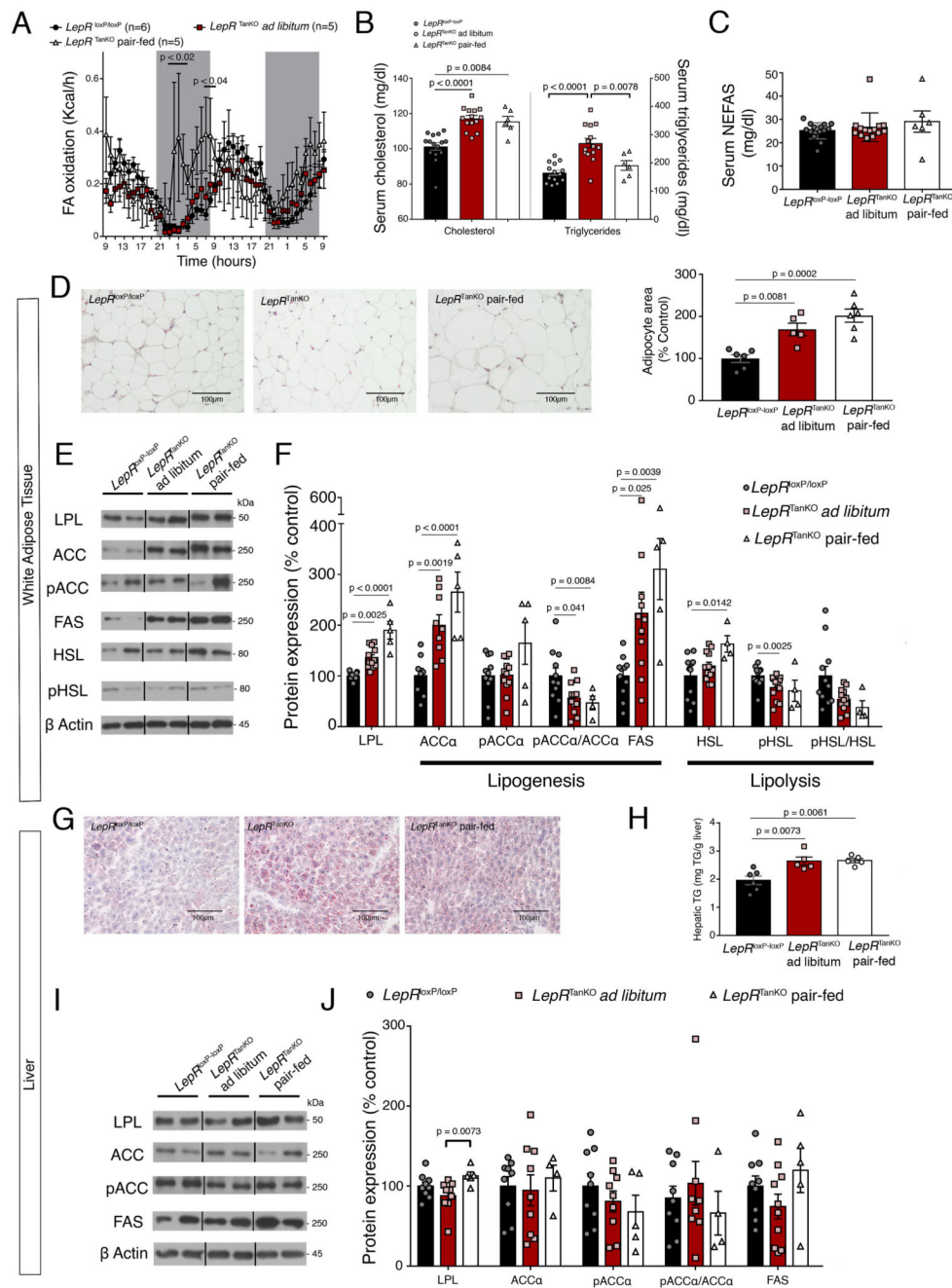


Figure 5. Selective *LepR* deletion in tanycytes causes hyperlipidemia and steatosis

(A) Fatty-acid (FA) oxidation over time. 2-way ANOVA with uncorrelated Fisher’s LSD test. Values indicate means \pm SEM; n indicates the number of mice.

(B) Graphs representing serum cholesterol and triglyceride concentrations in *LepR^{loxP/loxP}* and *LepR^{TanKO}* mice fed *ad libitum* on chow and *LepR^{TanKO}* mice pair-fed with *LepR^{loxP/loxP}* mice, 12 weeks after TAT-Cre infusion. One-way ANOVA with Tukey multiple comparison test or Kruskal-Wallis test with Dunn multiple comparison test were applied

depending Shapiro-Wilk normality test results. Values indicate means \pm SEM; each dot represents a mouse (n=15,14,6,14,14,6).

(C) Graph representing serum non-esterified fatty acid (NEFAS) concentrations in *LepR*^{loxP/loxP} and *LepR*^{TanKO} mice fed *ad libitum* on chow and *LepR*^{TanKO} mice pair-fed with *LepR*^{loxP/loxP} mice, 12 weeks after TAT-Cre infusion. One-way ANOVA with Tukey multiple comparison test. Values indicate means \pm SEM; each dot represents a mouse (n=15,14,6).

(D) Representative images of histological hematoxylin-eosin staining of the adipose tissue in *LepR*^{loxP/loxP} and *LepR*^{TanKO} mice fed *ad libitum* on chow and *LepR*^{TanKO} mice pair-fed with *LepR*^{loxP/loxP} mice illustrating quantifications in the graph. Graph shows quantification of adipocyte size. One-way ANOVA with Tukey multiple comparison test. Values indicate means \pm SEM; each dot represents a mouse (n=6,5,6).

(E) Representative western blots of the different proteins mentioned in (F).

(F) Graph representing protein expression levels of several proteins implicated in fatty acid synthesis or fatty acid lipolysis in white adipose tissue from *LepR*^{loxP/loxP} and *LepR*^{TanKO} mice, 12 weeks after TAT-Cre infusion. Lipoprotein lipase (LPL) is implicated in the lipids uptake from the circulation to the adipose tissue. One-way ANOVA with Tukey multiple comparison test or Kruskal-Wallis test with Dunn multiple comparison test. Values indicate means \pm SEM; each dot represents a mouse (n=11,12,5).

(G) Representative Oil-Red-stained images from the liver of *LepR*^{loxP/loxP} and *LepR*^{TanKO} mice fed *ad libitum* and *LepR*^{TanKO} mice pair-fed with *LepR*^{loxP/loxP} mice illustrating quantifications in H.

(H) Quantification of triglycerides in the liver of *LepR*^{loxP/loxP} and *LepR*^{TanKO} mice fed *ad libitum* and *LepR*^{TanKO} mice paired-fed with *LepR*^{loxP/loxP} mice. One-way ANOVA with Tukey multiple comparison test. Values indicate means \pm SEM; each dot represents a mouse (n=6,5,5).

(I) Representative western blots of the different proteins mentioned in (J).

(J) Graph representing protein expression levels of several proteins implicated in fatty acid synthesis and lipid uptake from the circulation into the liver in *LepR*^{loxP/loxP} and *LepR*^{TanKO} mice fed *ad libitum* and *LepR*^{TanKO} mice paired-fed with *LepR*^{loxP/loxP} mice, 12 weeks after TAT-Cre infusion. One-way ANOVA with Tukey multiple comparison test. Values indicate means \pm SEM; each dot represents a mouse (n=9,10,4).

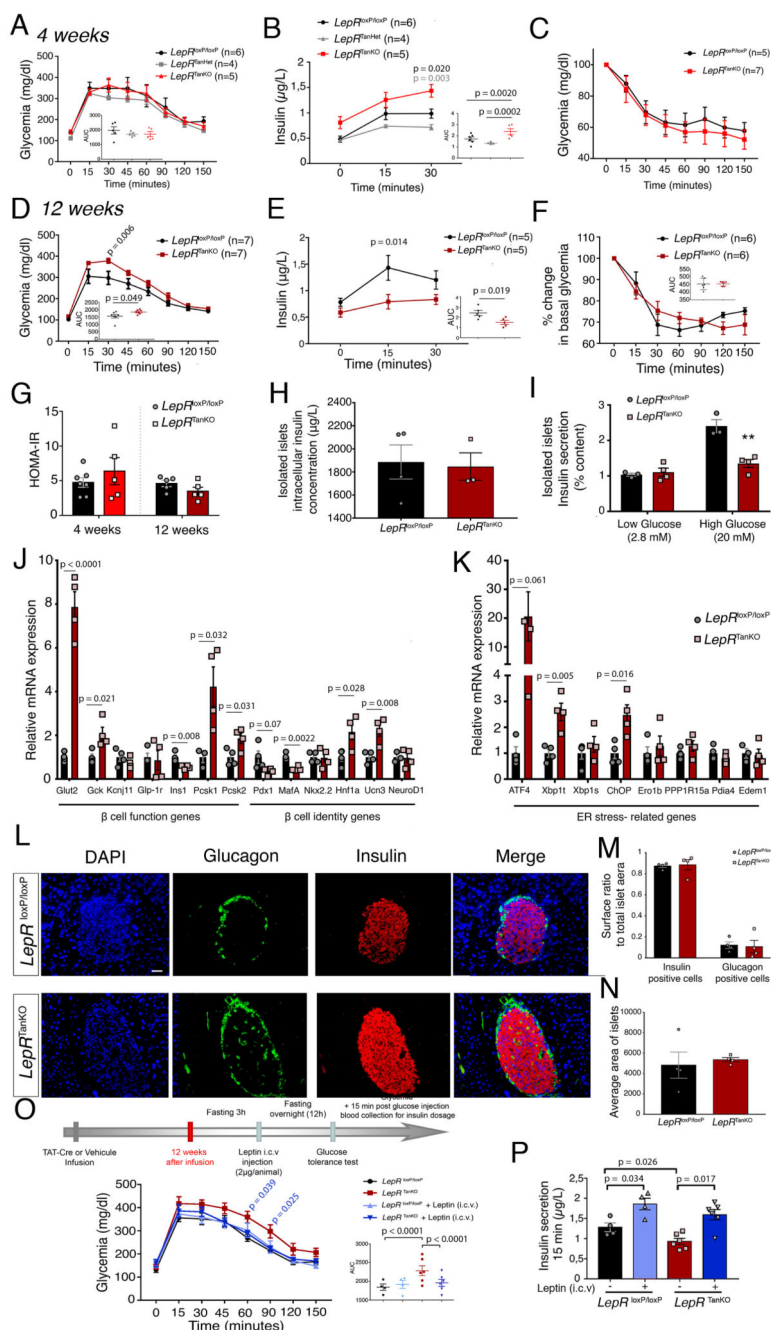


Figure 6. Loss of LepR expression in median eminence tanycytes causes severe pancreatic β cell dysfunction possibly due to defective noradrenaline activity

(A) Curve representing glycemia during a glucose tolerance test in *LepR^{loxP/loxP}*, *LepR^{TanHet}* and *LepR^{TanKO}* mice, 4 weeks after TAT-Cre infusion. Graph represents the area under the curve; two-way ANOVA with Tukey’s correction. Values indicate means ± SEM; n indicates the number of mice.

(B) Serum insulin concentrations during the first 30 mins of a glucose tolerance test in *LepR^{loxP/loxP}*, *LepR^{TanHet}* and *LepR^{TanKO}* mice, 4 weeks after TAT-Cre infusion; two-way

ANOVA with Tukey's correction. Values indicate means \pm SEM; n indicates the number of mice.

(C) Graph representing serum insulin concentrations at T0 of the glucose tolerance test; two-sided t-test. Values indicate means \pm SEM; n indicates the number of mice.

(D) Curve representing glycemia during a glucose tolerance test in *LepR*^{loxP/loxP} and *LepR*^{TanKO} mice, 12 weeks after TAT-Cre infusion; two-way ANOVA with Tukey's correction. Values indicate means \pm SEM; n indicates the number of mice.

(E) Serum insulin concentrations during the first 30 mins of a glucose tolerance test in *LepR*^{loxP/loxP} and *LepR*^{TanKO} mice, 12 weeks after TAT-Cre infusion; two-way ANOVA with Tukey's correction. Values indicate means \pm SEM; n indicates the number of mice.

(F) Percentage change in basal glycemia during an insulin tolerance test in *LepR*^{loxP/loxP} and *LepR*^{TanKO} mice, 12 weeks after TAT-Cre infusion. Two-way ANOVA with Sidak's multiple comparison (two-sided unpaired t-test for AUC, inset). Values indicate means \pm SEM; n indicates the number of mice.

(G) HOMA-IR. Two-sided unpaired t-test. Values indicate means \pm SEM; each dot represents a mouse (n=7,5,5,5).

(H) Graph representing insulin secretion from total isolated pancreatic islets from *LepR*^{loxP/loxP} and *LepR*^{TanKO} mice, 12 weeks after TAT-Cre infusion, following treatment with low or high glucose concentrations. Two-sided unpaired t-test. Values indicate means \pm SEM; each dot represents a mouse (n=3,4).

(I) Graph representing insulin concentrations in isolated pancreatic islets from *LepR*^{loxP/loxP} and *LepR*^{TanKO} mice, 12 weeks after TAT-Cre infusion. Two-way ANOVA with Tukey's multiple comparison. Values indicate means \pm SEM; each dot represents a mouse (n=3,4).

(J) Relative mRNA expression levels of markers of β -cell function and identity in isolated pancreatic islets from *LepR*^{loxP/loxP} and *LepR*^{TanKO} mice, 12 weeks after TAT-Cre infusion. A two-sided unpaired Student t-test or Mann-Whitney U test was applied, depending on Shapiro-Wilk normality test results. Values indicate means \pm SEM; each dot represents a mouse (n=4,4).

(K) Relative mRNA expression levels of ER stress markers in isolated pancreatic islets from *LepR*^{loxP/loxP} and *LepR*^{TanKO} mice, 12 weeks after TAT-Cre infusion. A two-sided unpaired Student t-test or Mann-Whitney U test was applied, depending on Shapiro-Wilk normality test results. Values indicate means \pm SEM; each dot represents a mouse (n=4,4).

(L) Representative confocal images representing nuclei (blue), glucagon (green) and insulin (red) in isolated pancreatic islets from *LepR*^{loxP/loxP} and *LepR*^{TanKO} mice, 12 weeks after TAT-Cre infusion illustrating quantifications in M. Scale bar: 50 μ m.

(M) Graphs representing the ratio between insulin-positive (left) or glucagon-positive area (right) to the total islet surface area in *LepR*^{loxP/loxP} and *LepR*^{TanKO} mice, 12 weeks after TAT-Cre infusion. Two-way ANOVA with Tukey's multiple comparison. Values indicate means \pm SEM; each dot represents a mouse (n=4,4).

(N) Graph representing the average surface area of pancreatic islets from *LepR*^{loxP/loxP} and *LepR*^{TanKO} mice, 12 weeks after TAT-Cre infusion. Mann-Whitney test. Values indicate means \pm SEM; each dot represents a mouse (n=4,4).

(O) Curve representing glycemia during a glucose tolerance test in *LepR*^{loxP/loxP} and *LepR*^{TanKO} mice, before (black and red curves) and after (light and dark blue curves) i.c.v. leptin injection (2 μ g/animal). Graph represents the area under the curve; one-way ANOVA with

Tukey's correction. Values indicate means \pm SEM. The n number of mice is identical in the main graph and bottom right graph, where each mouse is represented by a dot (n=4,4,6,6). **(P)** Serum insulin concentrations at 15 minutes during the glucose tolerance test presented in **(O)**. A paired two-sided t-test was applied for comparisons between the same group before and after leptin injection and a two-sided unpaired t-test. Values indicate means \pm SEM; each dot represents a mouse (n=4,4,6,6).

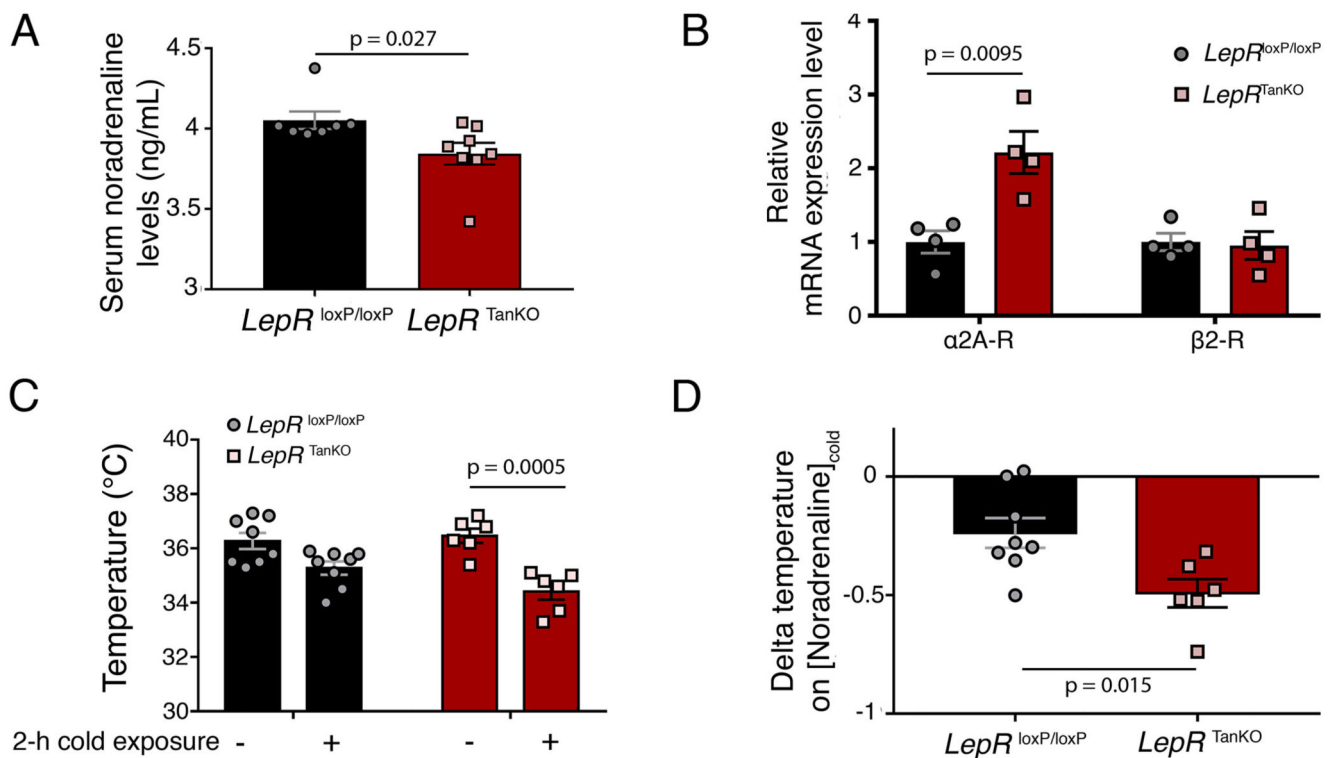


Figure 7. Loss of *LepR* expression in median eminence tanycytes alters adrenergic receptor expression in the pancreas and impairs cold-mediated increases in noradrenaline

(A) Serum noradrenaline concentrations in *LepR^{loxP/loxP}* and *LepR^{TanKO}* mice, 12 weeks after TAT-Cre infusion. Two-sided unpaired Student's t-test. Values indicate means \pm SEM; each dot represents a mouse (n=7,8).

(B) Relative mRNA expression levels of adrenergic receptors in isolated pancreatic islets from *LepR^{loxP/loxP}* and *LepR^{TanKO}* mice, 12 weeks after TAT-Cre infusion. Two-sided unpaired Student's t-test. Values indicate means \pm SEM; each dot represents a mouse (n=4 in each group).

(C) Rectal temperature measured in *LepR^{loxP/loxP}* and *LepR^{TanKO}* mice, 12 weeks after TAT-Cre infusion, before and after 2h cold exposure. Two-sided paired Student's t-test. Values indicate means \pm SEM; each dot represents a mouse (n=8,8,6,6).

(D) Ratio between the delta temperature after-before cold exposure to the serum noradrenaline concentration after cold exposure from *LepR^{loxP/loxP}* and *LepR^{TanKO}* mice. Two-sided unpaired Student's t-test. Values indicate means \pm SEM; each dot represents a mouse (n=8,6).

Table 1
Knocking out LepR in tanycytes blunts the leptin-mediated neuroendocrine response to fasting

	<i>LepR^{loxP/loxP}</i>			<i>LepR^{TanKO}</i>		
	Fed	Fasting + Saline	Fasting + Leptin	Fed	Fasting + Saline	Fasting + Leptin
	n=13	n=6	n=6	n=10	n=5	n=5
Blood glucose (mg.dl ⁻¹)		96.7 ± 1.9***	105.0 ± 4.7***	217.6 ± 7.5	97.4 ± 6.6***	107.0 ± 2.4***
Change in bodyweight after 24h refeeding (g)		1.92 ± 0.18	1.33 ± 0.19 ^{\$1}		1.08 ± 0.35	0.80 ± 0.37
Cumulative food intake after refeeding (g) 4h		1.35 ± 0.06	1.15 ± 0.04 ^{\$2}		1.28 ± 0.06	1.2 ± 0.08
12h		2.65 ± 0.13	2.07 ± 0.22 ^{\$3}		2.22 ± 0.19	1.98 ± 0.12
24h		6.07 ± 0.29	5.30 ± 0.28		5.60 ± 0.57	4.94 ± 0.26
Corticosterone (ng.ml ⁻¹)	38.1 ± 2.6	88.0 ± 9.9***	58.9 ± 5.9* ^{\$\$}	40.5 ± 3.8	57.5 ± 10.3	51.4 ± 6.9

Table summarizing data from fed and 24h fasting and refed *LepR^{loxP/loxP}* and *LepR^{TanKO}* mice after saline or leptin (1mg/kg) i.p injection. Two-sided unpaired Student's t-test or one-way ANOVA with Tukey's correction as required. ***: p<0.0001, *: p = 0.023 compared to fed mice; \$\$: p = 0.007, \$1: p = 0.049, \$2: p = 0.018, \$3: p = 0.045 compared with fasting mice treated with saline. Values indicate means ± SEM. n indicates the number of mice in each group.